Nonreciprocal Devices
Microwave Circuit Optomechanics

Integrated MSc. Thesis
10 December 2016

Akshay Koottandavida
UM-DAE Centre for Excellence in Basic Sciences, Mumbai

Thesis Advisor :
Prof. Tobias Kippenberg
laboratoire LPQM
École Polytechnique Fédérale de Lausanne

What I cannot create, I do not understand.
— Richard Feynman

In loving memory of Abhijith Varma. You left fingerprints of grace in our lives.
You shan't be forgotten....

Acknowledgements

I would first like to thank my thesis advisor Prof. Tobias Kippenberg of the LPQM laboratory at EPFL for giving me this opportunity to work under him and his extraordinary team. Prof. Kippenberg offered me his immense support, both professionally and financially and is a continuing source of inspiration for me. I am truly indebted to him for allowing me to be a part of his laboratory family and I sincerely hope that I was able to meet his expectations. I would also like to extend my sincere gratitude to Dr. Alexey Feofanov for his continued support of my thesis study, for his patience, motivation, and immense knowledge. His guidance helped me in all the time of research and writing of this thesis and he consistently allowed this paper to be my own work, but steered me in the right direction whenever he thought I needed it.

I would also like to acknowledge my fellow group members Daniel Toth and Nathan Bernier for the stimulating discussions and precious support which guided me through this study. I would like to express my sincere gratitude to my institute for supporting me during my time in Switzerland, being patient with me and for providing the freedom to complete this thesis at my own pace.

Finally, I must express my very profound gratitude to my parents, my colleague Naman Agarwal and to my closest friend Leah Chrestien for her valuable input, unfailing support and continuous encouragement throughout the duration of this study. This accomplishment would not have been possible without them. Thank you.

Lausanne, 10 December 2016 Akshay Koottandavida

Abstract

Reciprocity is the invariance in system response with respect to the exchange of source and detector. Non-reciprocal devices such as isolators play a key role in quantum information processing applications. Commercially available realisations of such devices rely on external magnetic bias rendering them unsuitable for superconducting quantum circuits and on-chip integration. We study the theoretical framework for magnetic bias-free non-reciprocal frequency conversion in multi mode microwave circuit optomechanics. The simplest coupled mode system, where all the couplings are optomechanical in nature, that can break reciprocal symmetry is a closed four mode scheme. We prove that such a system can, in theory, be operated as an ideal isolator. We also investigate several aspects involved in experimental realisation of the system as a result of which, a proof of concept has been effected [1] . Furthermore, we investigate and put forward a superconducting co-planar waveguide circuit design to implement non-reciprocity using reservoir engineering. Key idea behind this scheme is to engineer the mechanical damping rate so as to reach the reverse dissipation regime [2, 3] . Finally, we discuss the versatility of this design using which one can combine non-reciprocity and reverse dissipation regime to obtain much larger isolation bandwidth and also the possibility of optomechancial topological states.

Key words: non-reciprocal device, microwave circuit optomechanics, quantum engineering

Contents

Acknowledgements **i**

Abstract **iii**

List of figures **vi**

List of tables **vii**

Introduction **1**

1 Theoretical Foundations **3**
1.1 Basics of Resonator Optics 3
1.2 Cavity Optomechanics 4
1.3 Dynamical Backaction 6
1.4 Input-Output Formalism 6
1.5 Optomechanical Equations of Motion 7
1.6 Red detuned : Sideband Cooling 8
1.7 Blue detuned : Parametric Amplification 9
1.8 Resonant Drive 9
1.9 Microwave Circuit Optomechanics 10
1.9.1 Inductive Coupling to External Feedline 11
1.9.2 Capacitive Coupling to External Feedline 12

2 Schemes for Non-Reciprocity **13**
2.1 Definition of Reciprocity 13
2.2 Non-Reciprocity in a General Coupled Mode System 14
2.3 Reconfigurable Non-Reciprocal Device 16
2.4 Non-Reciprocity via Engineered Reservoir 16

3 Non-Reciprocity in OM Systems **19**
3.1 The Simplest System 19
3.1.1 Effective Decay Rates Matched 23
3.1.2 Cooperativities Matched 24
3.2 4-Mode System using Engineered Reservoir 25

4 Non-Reciprocity Implementation **29**
4.1 The Simplest System : 4 Modes 29
4.2 4-Mode Reverse Dissipation Regime Scheme 29

4.2.1 Constraints in Circuit Design 29
4.2.2 Circuit Details 30
4.2.3 External Coupling via Impedance Transformer 34

Conclusion **35**

A System Parameters **37**
A.1 Mathematica Simulations 37
A.2 Sonnet Simulations 38

Bibliography **40**

List of Figures

1.1 Fabry perot resonator 4
1.2 Canonical OM setup 5
1.3 Red Detuned 8
1.4 Circuit Optomechanics setup. 10
1.5 External Coupling Circuits 11

2.1 Reciprocity Definition 13
2.2 (a)Directed Graph (b) JPC non-reciprocity 15
2.3 Reverse Dissipation Regime 18

3.1 Diamond scheme 20
3.2 Scattering Matrix Elements for the Diamond Scheme 22
3.3 (a)Scattering Matrix Elements for no δ (b) Ratio of off-diagonal elements 23
3.4 Contour Plot of R 24
3.5 4 Mode RDR scheme 25
3.6 Scattering Matrix Elements for 4 Mode RDR Scheme 26
3.7 Scattering Matrix Elemtns for 4 Mode RDR Scheme 27

4.1 2D circuit 31
4.2 3D circuit 32
4.3 Circuit Response 32
4.4 Mode shape 33
4.5 Calculation of g_0 33
4.6 $\kappa_{ex}\, vs L$ 34

List of Tables

4.1 g_0 calculation 31

A.1 System Parameters 37
A.2 Sonnet Simulation parameters 38

Introduction

Symmetry of a physical system is the invariance of its characteristics under some transformations. For instance, classical electromagnetic theory defines reciprocity as the symmetry with respect to the exchange of current densities (sources) and the resulting fields generated at the detector(observer) [4]. A reciprocal system therefore exhibits an invariant response upon reversing the direction of signal propagation. Reciprocity can be advantageous in classical systems such as antennas where it enforces identical radiation and reception responses. Systems such as superconducting quantum circuits however, could benefit from non-reciprocal devices which maintains a preferred direction. Isolators, circulators and directional amplifiers for example, play a crucial role in signal routing and processing in qubit read-out circuits. Such commercial devices use magnetic materials and fields to implement a non-reciprocal rotation of polarization vector of light (Faraday rotation). Although broadband in its operation, these devices are extremely limited in their applicability to quantum systems mentioned above. Detrimental insertion losses and added noise can destroy the quantum coherence of microwave signals. Moreover, the use of magnetic materials renders these devices incompatible with superconducting circuits and on-chip integration. Fast advances in the field of quantum information processing and qubit technology in recent years spurred the investigation into alternative schemes to break reciprocal symmetry.

It was recently proposed that tuning a coherent interaction between two electromagnetic modes with a dissipative one, in a coupled mode system can help to achieve non-reciprocal propagation between ports [5, 6]. This novel concept has recently been experimentally realised in the field of circuit optomechanics, where microwave modes are coupled to mechanical oscillators, which act as the dissipative coupling [3]. The resonator enhanced interaction between the microwave and mechanical modes is inherently a non-linear one [7]. In this thesis we put forward the theory and design for implementing such a scheme in the regime of superconducting microwave circuit optomechanics. Moreover, we investigate conditions where the dissipation rate of the mechanical mode can be increased to a point where it acts as a cold reservoir for the electromagnetic modes in the Reverse Dissipation Regime. We study how to effectively utilise this regime to increase the bandwidth of non-reciprocity.

Another, more general theoretical proposition, predicates that coupled mode systems with dissipation can be tuned to achieve non-reciprocal propagation via the use of carrier waves(pumps) [8]. The different pathways within such a system can be made to interfere owing to the asymmetrical carrier phases picked up along each route by the signal. This interference can lead to non-reciprocal transmission(or amplification) with respect to the ports. A minimum of 3 coupled modes were proven to be necessary for the interference condition to hold. Using Josephson junctions, this scheme was realized in experiment in the microwave domain to devise reconfigurable non-reciprocal frequency conversion and directional amplification of signals [9]. Although robust, this scheme utilities a small magnetic bias to activate the interaction between the modes set up by the Josephson junction. Recently, we have seen implementations of such schemes in the optical regime as well [10, 11] . In this thesis we present the theoretical framework and the consequent proof of concept for a fully magnetic-free non-reciprocal device using multi mode circuit optomechanics. The system under consideration is a highly symmetric closed four mode scheme in which all the couplings are optomechanical in nature. The proposed scheme is a subset of the coupled mode framework mentioned above. Near ideal isolation between the ports(frequencies of the modes) is achieved by using a unique combination of pump frequencies which leads to interference of the frequency conversion Lorentzian features between the modes. Further studies into the scheme can provide deeper insights, more robust implementation and much larger bandwidth for commercial use in the future.

1 Theoretical Foundations

This chapter of the thesis is intended to give an introduction to the basic concepts of non-reciprocal devices, cavity optomechanics and circuit optomechanics. As the name suggests, cavity optomechanics deals with the interaction between light and mechanics in an optical cavity. Specifically, a mechanical resonator coupled to light field inside a cavity.

1.1 Basics of Resonator Optics

We will first review the classical dynamics of light field inside a Fabry-Perot resonator as shown in fig. 1.1. The allowed modes inside the resonator can be calculated by a traveling wave approach. That is, we imagine the cavity modes as bouncing back and forth between the cavity mirrors. We say that after one round trip of the cavity, the phase picked up by a wave is an integer multiple of 2π.

$$\phi = \mathrm{k}\,2L = 2\pi j, \tag{1.1}$$

where j is a positive integer (mode number). With this condition, the cavity will sustain self reproducing waves. Therefore one can find the resonance frequencies of the allowed cavity modes as,

$$\omega_{\mathrm{cav},j} = \frac{j\pi c}{L} \tag{1.2}$$

where c is the speed of light in the medium and L is the cavity length. Hence the spectra of the resonator contains a series of equally spaced resonances with a separation between given by the Free Spectral Range (FSR) of the cavity : $\Delta\omega_{FSR} = \pi\frac{c}{L}$. The finite mirror transmission and the internal absorption or scattering out of the cavity leads to a finite photon lifetime inside the cavity, τ, with the photon decay rate defined as $\kappa = \tau^{-1}$. A further useful quantity is the optical finesse, F, which gives the average number of round-trips a photon makes before it leaves the cavity. This is defined as :

$$F = \frac{\Delta\omega_{\mathrm{FSR}}}{\kappa} = \tau\Delta\omega_{\mathrm{FSR}} \tag{1.3}$$

Alternatively, one can define the Quality factor (Q) of the cavity : $Q = \Delta\omega_{\mathrm{cav}}\tau$. The Q factor characterizes the resonator's bandwidth relative to its center frequency. A higher Q indicates lower energy loss rate relative to the total stored energy of the resonator. This means that the oscillations die out more slowly. The decay rate (κ) can have two main contributions. The external decay rate κ_{ex} characterizes the loss

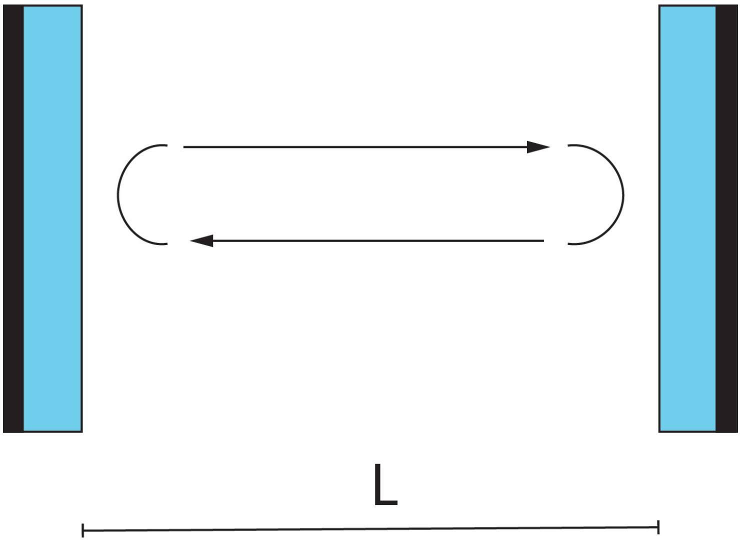

Figure 1.1 – Traveling waves sustained in a Fabry perot resonator of length L. The blue shaded region represents the reflective part or the mirrors.

associated with the interface between an incident light and the mirror while κ_{in} summarizes the decay rate inside the cavity, including transmission losses at the second mirror, scattering and absorption losses behind the first mirror. Hence, for a high Q cavity, the total cavity loss can be expressed as

$$\kappa = \kappa_{\text{ex}} + \kappa_{\text{in}} \tag{1.4}$$

The coupling efficiency to the cavity is given by $\eta = \frac{\kappa_{\text{ex}}}{\kappa}$. Now let us look at the quantum treatment of this system. The system can be modeled as a quantum harmonic oscillator with different modes representing equally spaced energy levels. The photons in the fundamental mode has frequency ω_{cav}, with $\hat{a}$ and $\hat{a}^\dagger$, the bosonic annihilation and creation operators obeying commutation relation $[\hat{a}, \hat{a}^\dagger] = 1$. The modes have energy given by :

$$E_j = \hbar\omega_{\text{cav},j}\left(\hat{a}^\dagger\hat{a} + \frac{1}{2}\right) = \hbar\omega_{\text{cav},j}\left(\hat{n} + \frac{1}{2}\right) \tag{1.5}$$

where $\hat{n}$ is the number operator. A photon striking a mirror will exert a radiation force on it, due to its momentum. This force is typically extremely small to have any observable effect. But using a cavity such as the one described above, the photons, which are trapped, will strike the mirror repeatedly thereby enhancing the force experienced by the mirror. The effects of these forces can be studied by using a movable mirror in place of a stationary one.

1.2 Cavity Optomechanics

Fig. 1.2 represents a canonical cavity optomechanical system in which one of the mirrors of a Fabry-Perot resonator is coupled to a mechanical spring. First let us consider an idealized system where the mechanical oscillator is initially stationary. When photons enter the cavity and strike the movable mirror, it imparts a radiation pressure force [7, 12] on the mechanical oscillator which in turn disturbs the mirror from its equilibrium position [13] . Consequently, the mirror starts oscillating with a frequency Ω

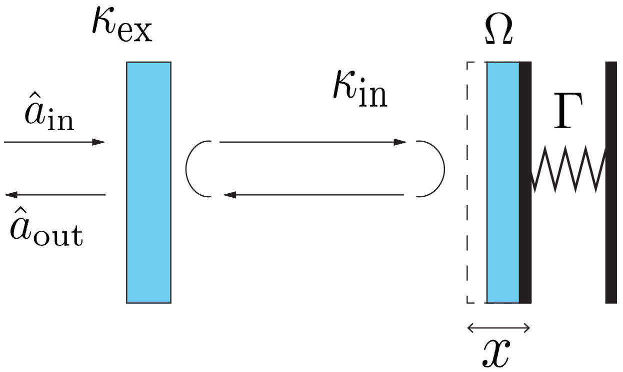

Figure 1.2 – Depiction of a canonical OM setup showing the input($\hat{a}_{\text{in}}$) and output($\hat{a}_{\text{out}}$) signals and the internal(κ_{in}) and external(κ_{ex}) decay rates for the EM mode. The end mirror oscillates due to radiation pressure force with a frequency Ω and is modeled as a harmonic oscillator with decay rate Γ. Due to this motion, the cavity length is modulated by a small amount x.

which changes the cavity length by $L(x) = L - x$, where x is the mechanical oscillator displacement from its equilibrium position. Hence the mode frequencies will be shifted as

$$\omega_{\text{cav},j}(x) = j\frac{\pi c}{L(x)} \simeq \frac{j\pi c}{L}\left(1+\frac{x}{L}\right) = \omega_{\text{cav},j}\left(1+\frac{x}{L}\right) \tag{1.6}$$

This approximation is valid as long as $x \ll L$, which is appropriate for the vast majority of cavity optomechanical systems. Hence we see that, to first order, the motion of the mechanical oscillator acts to linearly shift the optical resonance frequency. The optomechanical coupling strength G is defined as :

$$G = \frac{\mathrm{d}\omega_{\text{cav},j}(x)}{\mathrm{d}x} \tag{1.7}$$

For the above described Fabry-Perot resonator, with a movable mirror, we have $G = \frac{\omega_{\text{cav}}}{L}$. We can describe the mechanical oscillator using the raising and lowering operators just as we did with the intra cavity modes. This would allow us to view the interaction between light field and mechanical oscillator as two coupled harmonic oscillators. Now we can write the Hamiltonian of the combined system as :

$$\hat{H} = \hbar\omega_{\text{cav}}(\hat{x})\,\hat{a}^\dagger\hat{a} + \hbar\Omega\hat{b}^\dagger\hat{b} \tag{1.8}$$

Here, $\hat{b}$ and $\hat{b}^\dagger$ are the bosonic operators for mechanical excitations obeying the commutation relation $[\hat{b}, \hat{b}^\dagger] = 1$. Position operator $\hat{x}$ is defined as $\hat{x} = x_{\text{zp}}(\hat{b} + \hat{b}^\dagger)$ where $x_{\text{zp}} = \sqrt{\frac{\hbar}{2m\Omega}}$ is the zero point fluctuations. Expanding out Hamiltonian in equation eq. (1.8), we get (only considering the fundamental mode):

$$\hat{H} = \hbar\omega_{\text{cav}}\hat{a}^\dagger\hat{a} + \hbar\Omega\hat{b}^\dagger\hat{b} + \hbar g_0\hat{a}^\dagger\hat{a}\left(\hat{b}^\dagger + \hat{b}\right) \tag{1.9}$$

where $g_0 = Gx_{\text{zp}}$ is the *vacuum optomechanical coupling strength.* It is the optical frequency shift induced by a mechanical displacement equal to the mechanical zero-point motion. Hence optical cavity response is modified due to the presence of a mechanical oscillator. One can now see the formation of sidebands in the cavity spectrum, spaced out at the mechanical oscillator frequency.

In the majority of optomechanical experiments, the optical cavity resonance frequency ω_c, is much larger than all other system rates, such as mechanical oscillator frequency. Hence, in this regime, it is convenient to move into a rotating frame at the incident laser field ω_l and thereby remove the fast oscillations of the optical field. To do this, we perform the transformation $\hat{a} \rightarrow e^{-i\omega_L t}\hat{a}$, to get the new Hamiltonian in the rotating frame as

$$\hat{H}_{\text{rot}} = -\hbar\Delta\hat{a}^\dagger\hat{a} + \hbar\Omega\hat{b}^\dagger\hat{b} - \hbar g_0\hat{a}^\dagger\hat{a}\left(\hat{b} + \hat{b}^\dagger\right) \tag{1.10}$$

Here $\Delta = \omega_{\text{cav}} - \omega_{\text{L}}$, is the detuning between optical cavity and the incident laser frequency.

1.3 Dynamical Backaction

The Hamiltonian of the system described in the previous section reveals that the interaction between the movable mirror and radiation field is fundamentally a nonlinear process, involving 3 operators. The radiation pressure force [14], which is simply the derivative of the interaction Hamiltonian, is therefore given by

$$\hat{F} = -\frac{\mathrm{d}\hat{H}}{\mathrm{d}x} = \hbar g\hat{a}^\dagger\hat{a} \tag{1.11}$$

The mechanical motion induces a shift of the optical resonance frequency, which changes the intensity of circulating light and therefore, of the radiation pressure force acting on the oscillator. Such a feedback loop is known as optomechanical backaction. But due to the finite cavity decay rate κ, there exists some retardation between the motion and the resulting changes in force. Hence it is labeled as *Dynamical Backaction.* To study the effects of this dynamical backaction, we start from the input-output formalism which will provide us with the equations of motion of the system.

1.4 Input-Output Formalism

In this approach, we consider our system (cavity modes) coupled to a heat bath (external field) [15, 16]. Our aim is to determine the effect of intra cavity dynamics on the quantum statistics of the output filed. Within this perspective, we will also treat the field input to the cavity explicitly. The system we will consider is that of a single cavity mode interacting with an external multi-mode field (bath). We can write the total Hamiltonian(in RWA) without explicitly defining the system as :

$$\hat{H} = \hat{H}_{\text{sys}} + \hat{H}_{\text{bath}} + \hat{H}_{\text{int}} \tag{1.12}$$

where,

$$\hat{H}_{\text{bath}} = \hbar\int_{-\infty}^{\infty} \omega\,\hat{a}^\dagger(\omega)\,\hat{a}(\omega)\,\mathrm{d}\omega \tag{1.13}$$

$$\hat{H}_{\text{int}} = i\hbar\int_{-\infty}^{\infty} \kappa(\omega)\left[\hat{a}^\dagger(\omega)\hat{c} - \hat{c}^\dagger\hat{a}(\omega)\right]\mathrm{d}\omega \tag{1.14}$$

Note that the above mentioned operators are time dependent and obey the commutation relation $[\hat{a}(\omega), \hat{a}(\omega')] = \delta(\omega - \omega')$. Here $\kappa(\omega)$ is the frequency dependent damping rate and we chose to make the *First Markov Approximation* which states that :

$$\kappa(\omega) = \sqrt{\frac{\gamma}{2\pi}} \tag{1.15}$$

It says that the damping rate is independent of frequency over a wide range of frequencies around $\omega = 0$ (i.e. around $\omega = \omega_l$ in non-rotating frame). As the system is confined, we need to determine how the field outside responds to the presence of system and any matter it may contain. We say that $\hat{c}$ and $\hat{d}$ are two of the several possible system modes. Now we follow standard procedure [] and derive the Heisenberg equations of motion for $\hat{a}(\omega)$ and $\hat{d}$ in the interaction picture. We also define an input field to obtain the *Quantum Langevin Equation* (QLE) in the rotating frame of light :

$$\dot{d} = -\frac{i}{\hbar}[d, H_{\text{sys}}] - \left[[d, c^\dagger] \left\{ \frac{\gamma}{2} c + \sqrt{\gamma} a_{\text{in}}(t) \right\} - \left\{ \frac{\gamma}{2} c^\dagger + \sqrt{\gamma} a^\dagger_{\text{in}}(t) \right\} [d, c] \right] \tag{1.16}$$

Assuming $t_1 > t$, one can also solve equation Heisenberg equation by defining an output field to get the time reversed QLE. By comparison, one arrives at the *input-output* relation :

$$a_{\text{out}}(t) = a_{\text{in}}(t) + \sqrt{\gamma} c(t) \tag{1.17}$$

Using the Quantum Langevin Equation and the Input-Output relation, one can set up the equations of motion for our system.

1.5 Optomechanical Equations of Motion

Now we move on to write the optomechanical equations of motion [14] for the cavity field $\hat{a}$ and the mechanical mode $\hat{b}$. These equations have the form of quantum Langevin equations since both the light amplitude and the mechanical motion are driven by the noise terms (vacuum noise and any thermal noise entering the system). κ and Γ are the decay rates of the optical and mechanical modes respectively. We substitute the system Hamiltonian (in the rotating frame of incident light) into the QLE (eq. (1.16)) and derive the equations of motion for the two system modes :

$$\dot{a} = \left(i\Delta - \frac{\kappa}{2} \right) a + i g_0 a (b + b^\dagger) - \sqrt{\kappa} a_{\text{in}} \tag{1.18}$$

$$\dot{b} = -\left(i\Omega + \frac{\Gamma}{2} \right) b + i g_0 a^\dagger a - \sqrt{\Gamma} b_{\text{in}} \tag{1.19}$$

From the steady state solution of eq. (1.18), we obtain the mean intra cavity photon occupation as [13]:

$$\bar{n}_{\text{cav}} = |\bar{a}|^2 = \frac{\kappa}{(\frac{\kappa}{2})^2 + [\Delta + g_0(b + b^\dagger)]^2} \frac{P_{\text{in}}}{\hbar\omega_L} \tag{1.20}$$

where P_{in} is the total power of the incident light(frequency ω_L) defined as $P_{in} = \hbar\omega_L n_{\text{in}}$ and $n_{\text{in}} = \langle a^\dagger_{\text{in}} a_{\text{in}} \rangle$ is the number of photons incident on the cavity. The equations of motion eq. (1.18) and eq. (1.19) are inherently nonlinear as they contain the product of mechanical oscillator amplitude and

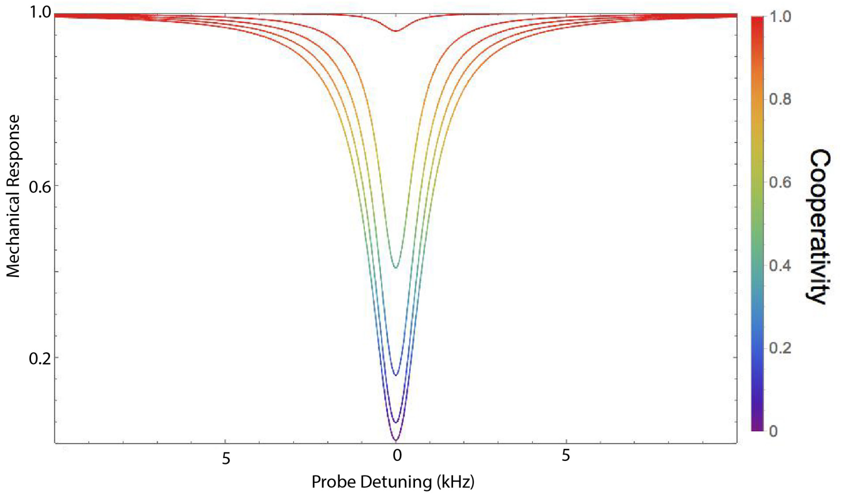

Figure 1.3 – Modification of mechanical decay rate with pump power due to red detuned pump [14].

the cavity field. For the quantum regime, they cannot be solved exactly in this form. However, we assume that the system has reached steady state due to a strong coherent laser drive(of amplitude α) and we study the linearized dynamics of the fluctuations on top of this drive. Therefore, linearizing the Hamiltonian by setting $\hat{a} = \alpha + \delta\hat{a}e^{i\Delta t}$, we get :

$$\hat{a}^\dagger\hat{a} = \alpha^2 + \alpha\left(e^{i\Delta t}\delta\hat{a} + e^{-i\Delta t}\delta\hat{a}^\dagger\right) + \delta\hat{a}^\dagger\delta\hat{a} \tag{1.21}$$

We neglect the last term, (much smaller than the second for large drive) and the first term (which leads to a constant radiation pressure force which simply shifts the resonator's equilibrium position). We also move into the interaction picture by making the transformation $\hat{b} \to \hat{b}e^{-i\Omega t}$. Thus we obtain the Hamiltonian of linearized optomechanical system :

$$\hat{H}_{\text{lin}} \approx -\hbar\Delta\delta\hat{a}^\dagger\delta\hat{a} - \hbar g\left(e^{i\Delta t}\delta\hat{a} + e^{-i\Delta t}\delta\hat{a}^\dagger\right)\left(\hat{b}^\dagger e^{i\Omega t} + \hat{b}e^{-i\Omega t}\right) \tag{1.22}$$

where $g = g_0\alpha = g_0\sqrt{\bar{n}_{\text{cav}}}$. Such an approximation is valid for many of the situations that we will describe. Now for particular choice of detunings, the Hamiltonian can be made time independent and we can observe some interesting phenomena.

1.6 Red detuned : Sideband Cooling

For $\Delta = -\Omega$, we expand the quadratic term in the Hamiltonian and perform a Rotating Wave Approximation (RWA) to neglect the terms which has any time dependence(or fast oscillating terms). The Hamiltonian, therefore, reduces to one which resembles a *beam splitter* or *hopping interaction.*

$$\hat{H}_{\text{int}} = \hbar\Omega\delta\hat{a}^\dagger\delta\hat{a} - \hbar g(\delta\hat{a}\hat{b}^\dagger + \delta\hat{a}^\dagger\hat{b}) \tag{1.23}$$

This particular choice of Δ means that the incident drive photons have frequency (and hence energy) less than the cavity resonance. Hence the input photons need to absorb one quanta of phonon energy (annihilate one phonon) in order to become resonant with the cavity. This leads to decrease in phonon number and hence, cooling of the mechanical oscillator [17].

$$E_\mathrm{l} = \hbar\omega_\mathrm{l} = \hbar\omega_\mathrm{c} - \hbar\Omega = E_\mathrm{cav} - E_\mathrm{phonon} \tag{1.24}$$

One can write the equations of motion in this regime, in matrix form as :

$$\frac{\mathrm{d}}{\mathrm{dt}}\begin{bmatrix} \delta\hat{a} \\ \hat{b} \end{bmatrix} = \begin{bmatrix} -\left(i\Omega + \frac{\kappa}{2}\right) & ig \\ ig & -\left(i\Omega + \frac{\Gamma}{2}\right) \end{bmatrix}\begin{bmatrix} \delta\hat{a} \\ \hat{b} \end{bmatrix} - \begin{bmatrix} \sqrt{\kappa} & 0 \\ 0 & \sqrt{\Gamma} \end{bmatrix}\begin{bmatrix} \delta\hat{a}_{in} \\ \hat{b}_{in} \end{bmatrix} \tag{1.25}$$

Since the above matrix equation is of the form $\dot{v} = Mv - Kv_{in}$, we can solve this system in the frequency space by defining $v[\omega] = F[v]$ (and similarly for others variables), where F denotes the Fourier transform. Therefore,

$$-i\omega\mathscr{I}v[\omega] = Mv[\omega] - Kv_{in}[\omega] \tag{1.26}$$

where $\mathscr{I}$ is the identity matrix. Now the above equation along with the input-output relation, together gives $v_{out}[\omega] = S\,v_{in}[\omega]$, where

$$S = \mathscr{I} + K(M + i\omega\mathscr{I})^{-1}K \tag{1.27}$$

is the mode scattering matrix which relates the input field to the output field. We can now look at the linear response of the mechanical mode in the red detuned regime [14] [18, 19, 20] . A useful parameter to gauge the strength of the pump power is the *Cooperativity*, defined as $\mathscr{C} = 4g^2/\kappa\Gamma$. The mechanical response $|S_{22}|^2$ is a Lorentzian with the linewidth characterizing mechanical decay rate(Γ). Therefore, widening of the response corresponds to an increase in the effective decay rate of the oscillator. Due to higher decay rate, the mechanical oscillations will be suppressed faster, and hence the oscillator is being cooled.

1.7 Blue detuned : Parametric Amplification

For $\Delta = \Omega$ or the blue detuned case, photons entering the cavity will have energy higher than the intracavity photons. Hence, in order to become resonant with the cavity, these photons will lose energy to the mechanical oscillator. Therefore, we see heating of the mechanics. The resonant terms in the Hamiltonian, in RWA, resemble the *parametric amplification* operator.

$$\hat{H}_{int} = -\hbar\Omega\delta\hat{a}^\dagger\delta\hat{a} - \hbar g(\delta\hat{a}\hat{b} + \delta\hat{a}^\dagger\hat{b}^\dagger) \tag{1.28}$$

In this case the mechanical and optical modes are entangled [21, 22] . Positive detuning can also lead to parametric amplification and instability.

1.8 Resonant Drive

In this case of driving on resonance, one cannot neglect any terms in the interaction Hamiltonian : $\hat{H}_\mathrm{int} = -\hbar g(\hat{b}^\dagger + \hat{b})(\delta\hat{a} + \delta\hat{a}^\dagger)$. Due to the mechanical displacement, the cavity length is shifted which shifts the cavity modes. This translates into a phase shift in the output field. Hence, in this regime the cavity serves as an interferometer and can be used to measure very small displacements, similar to the

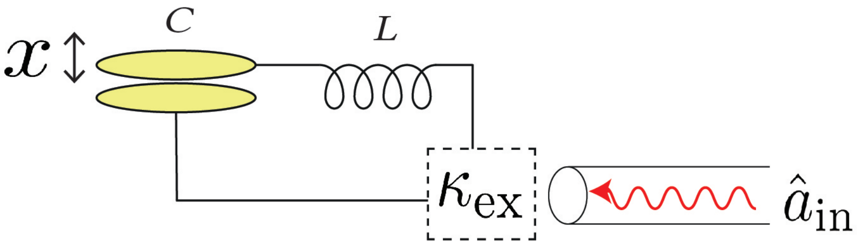

Figure 1.4 – Canonical circuit optomechanics setup where the mechanical element is a parallel plate drum capacitor in which the top plate is free to move. This changes the capacitance of the circuit thus coupling mechanical motion with the microwave signal. L and C are the inductance and the equilibrium capacitance of the circuit. The circuit can be coupled externally via mechanisms such as capacitive or inductive coupling with a decay rate of $\kappa_{\rm ex}$

setup used in LIGO in the detection of gravitational waves.

1.9 Microwave Circuit Optomechanics

In the previous section, we described the canonical optomechanical system in the optical regime. One can also set up such a system using LC circuits, in order to realise optomechanical interactions using microwave modes. An LC circuit, also called a resonant circuit, is an electric circuit consisting of an inductor and a capacitor connected together. It acts as an electrical resonator that stores energy oscillating at the circuit's resonant frequency $\omega_{\rm c} = \frac{1}{\sqrt{LC}}$. Therefore, such a circuit is analogous to an optical cavity in many ways. The mechanical element can be introduced in various ways in order to realise an optomechanical system. In this thesis, we will focus on the system developed in [23] , where one of the plates of the parallel plate capacitor used in the circuit, is suspended and allowed to freely oscillate (Ω). Due to this motion, capacitance of the circuit is modified, which leads to change in resonance frequency of the circuit. The optomechanical coupling rate is then calculated as,

$$g_0 = Gx_{\rm zp} = \frac{{\rm d}\omega}{{\rm d}x} x_{\rm zp} \tag{1.29}$$

Assuming that the mechanical element in this system is a movable parallel plate capacitor, the capacitance is modified as $C = \varepsilon_0 \frac{A}{d+x}$, where d is the equilibrium position of the capacitor plate, A is the area of the plates and ε_0 is the permittivity of air (medium between the plates). For $x << d$, therefore, the vacuum optomechanical coupling strength is

$$g_0 = \frac{\Delta\omega}{\Delta C} \frac{C_0}{d} x_{\rm zp} \tag{1.30}$$

where C_0 is the equilibrium capacitance of the capacitor, $\Delta\omega$ and ΔC corresponds to the change in frequency and capacitance due to mechanical motion respectively. Now that the system is defined, we proceed to study the coupling of a simple LC circuit to the external feedline. In an optical setup, the input signal can be coupled to the system via direct laser signal incident on the cavity [24] , evanescent coupling from a fiber [25] etc. In microwave experiments, the input signal from the external feedline can be coupled to the circuit (and intra cavity modes coupled to the external feedline) inductively or capacitively.

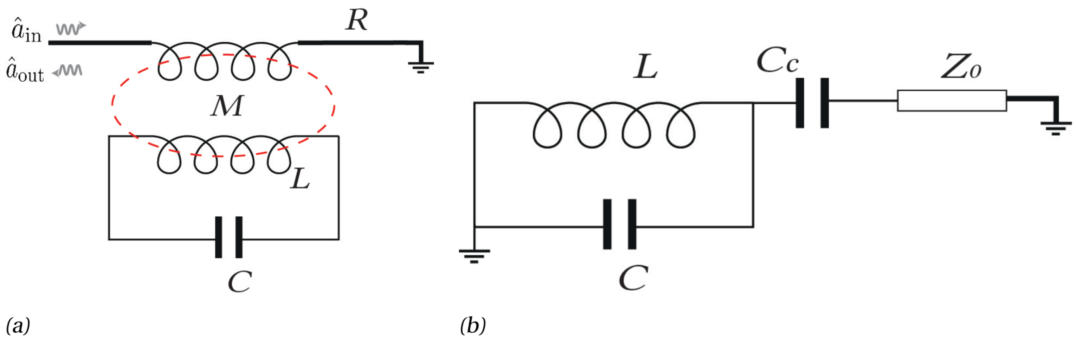

Figure 1.5 – (a)Basic LC circuit coupled inductively to an external feedline with mutual inductance M and termination impedance R. (b) An LC resonator capacitively coupled to an external feedline via an impedance transformer with characteristic impedance Z_0.

1.9.1 Inductive Coupling to External Feedline

Consider an LC resonator coupled to an external feedline(another Inductor) which is terminated at one end (Single Port Cavity). Let the resonator have an effective inductance and capacitance of L and C respectively. R is the termination impedance and M is the mutual inductance between the resonator inductor and the external feedline (fig. 1.5(a)). Consider an oscillating current $I(t) = I_0 cos(\omega t)$, flowing in the resonator. Total energy stored in the resonator is, therefore,

$$E_{\text{tot}} = \frac{LI_0^2}{2} \tag{1.31}$$

The average power loss per cycle to the external feedline is :

$$P = \langle \frac{V^2}{R} \rangle = \frac{M^2}{R} \langle \left(\frac{\mathrm{d}I}{\mathrm{dt}} \right)^2 \rangle = \frac{M^2 I_0^2 \omega^2}{2R} \tag{1.32}$$

The Q-Factor of the system is defined as the ratio of energy stored to energy dissipated per cycle.

$$Q = 2\pi \frac{E_{\text{tot}}}{E_{\text{dis}}} = \omega \frac{E_0}{P} \tag{1.33}$$

The external coupling rate, defined via the Q-factor as $\kappa_{\text{ex}} = \frac{\omega}{Q}$ becomes,

$$\kappa_{\text{ex}} = \frac{M^2 \omega^2}{LR} \tag{1.34}$$

For a double port cavity, the resonator will see two termination impedances in series, in the external feedline. Hence the effective impedance of the feedline becomes 2R. Therefore, the external coupling will be modified to

$$\kappa_{\text{ex}} = \frac{M^2 \omega^2}{2LR} = \frac{1}{2} \left(\frac{M}{L} \right)^2 \frac{1}{RC} \tag{1.35}$$

1.9.2 Capacitive Coupling to External Feedline

In the previous case, where the circuit was coupled inductively to the external feedline, the coupling strengths arise from the geometry of the modes themselves. A more robust method to control the mode coupling is by allowing a capacitor to mediate the coupling to the external feedline. An impedance transformer of suitable length, matching the impedances of different modes with respect to the feedline, along with coupling capacitors are used to selectively couple modes to the output ports. Consider an LC circuit coupled capacitively to an external active loss channel fig. 1.5. κ_{ex} for this system is given by,

$$\kappa_{\text{ex}} = \frac{1}{R(C + C_{\text{c}})} \tag{1.36}$$

where C_0 is the effective capacitance of the LC circuit (or one of the modes), C_{c} is the coupling capacitance and R is the impedance associated with the active element. Hence in order to tune κ_{ex} of the circuit, one can change the impedance of the active element using an impedance transformer (with impedance Z_{in} replacing R), which matches the impedance seen by the modes. In a series LC, the total admittance ($Y = \frac{1}{Z}$) of the circuit is :

$$Y_{\text{series}} = \frac{1}{\frac{1}{i\omega C_c} + Z_{in}} \tag{1.37}$$

where Z_{in} is the transformed impedance expressed in terms of load impedance $Z_{\mathscr{L}}$, characteristic impedance of the transformer Z_0, length of the transformer $\mathscr{L}$, speed of light in the medium v and frequency ω as

$$Z_{\text{in}} = Z_0 \frac{Z_{\mathscr{L}} + iZ_0 \tan\left(\frac{\omega\mathscr{L}}{v}\right)}{Z_0 + iZ_{\mathscr{L}} \tan\left(\frac{\omega\mathscr{L}}{v}\right)} \tag{1.38}$$

The above circuit is converted into a parallel LC and the admittances are matched to obtain equivalent impedances and capacitances, R_{eq} and C_{eq} respectively. By separating the real and imaginary parts one can obtain the equivalent capacitance and impedance :$Y_{\text{par}} = \frac{1}{R_{\text{eq}}} + i\omega C_{\text{eq}}$. Therefore the external coupling rate for a parallel LC circuit is given by

$$\kappa_{ex} = \frac{1}{R_{\text{eq}}(C + C_{\text{eq}})} \tag{1.39}$$

Therefore, by tuning the length of the impedance transformer, it is possible to control the external coupling of the modes. The use of this technique is shown in section 4.2.3.

2 Schemes for Non-Reciprocity

In this chapter we will discuss some of the proposed theoretical schemes for achieving non-reciprocal response without using external magnetic fields.

2.1 Definition of Reciprocity

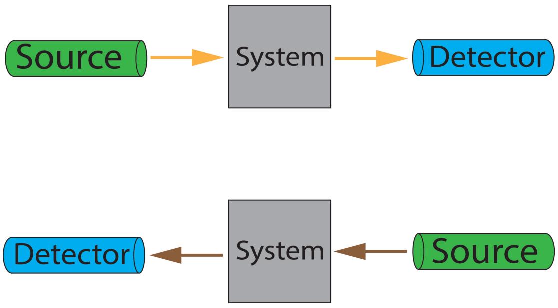

Figure 2.1 – Under a change of source and detector (observer), if the system perform identically, then it is possesses reciprocal symmetry.

First we will review the basic definition of reciprocity via the scattering matrix platform. A system is said to possess reciprocal symmetry if it responds invariantly under the exchange of source and observer (fig. 2.1). One can describe the system dynamics, say of device with two inputs and two outputs, as scattering of signals between the ports. In such a case, we can write down the scattering matrix which relates the source field to that at the detector.

$$\hat{a}_{\text{out}} = S\,\hat{a}_{\text{in}} \tag{2.1}$$

where S is a 2×2 matrix in this case. While the diagonal terms represents reflection from the ports, the off-diagonal terms indicate scattering from one port to the other. Reciprocal symmetry dictates that these off-diagonal terms be identical for the system. Consequently, a non-reciprocal system will have the condition $|S_{21}| \neq |S_{12}|$,since the scattering matrix elements can, in general, be complex. The off-diagonal elements can differ by a phase factor, but this can be eliminated by a redefinition of the input modes. This criterion can be generalised for an N-port device. For a passive system, where the input and output ports have the same frequencies, the condition for reciprocity states

$$S^T = S \tag{2.2}$$

where S^T is the transpose of S [26]. However, for an active device, with different frequency channels, the off-diagonal scattering elements pick up non-symmetric phases and thus the condition becomes even more general. The scattering matrix describes a fully reciprocal system if it obeys, in a suitable mode basis, the general constraint [8],

$$S^T = U_\phi S U_\phi^\dagger \tag{2.3}$$

where the unitary matrix $U = Diag\left[e^{i\phi_j}\right]$ with ϕ_js being the carrier phases which drives the signals and we can assume, without loss of generality, that $\sum \phi_j = 0$ where $j = 1,2,..,N$

2.2 Non-Reciprocity in a General Coupled Mode System

We will follow the description as given in [8] . Consider a 3 mode system, with angular frequencies ω_j and total dissipation rates γ_j, where the j^{th} mode is coupled to the k^{th} one with a coupling rate g_{jk} $(g_{jk} = \pm g^*_{kj};\, j \neq k;\, j,k \in \{1,2,3\})$. From the quantum Langevin equations of the modes (eq. (1.16))

$$\frac{\mathrm{d}v}{\mathrm{d}t} = -iHv + Kv_{in} \tag{2.4}$$

and the input-output relations (eq. (1.17)), one can derive the expression for scattering matrix (in frequency space) which relates the input fields to the output.

$$S = I + KM^{-1}K \tag{2.5}$$

Here, $v_{\text{out}} = S\, v_{\text{in}}$ where, S is the scattering matrix, $v_{\text{in}} = \left(a_{\text{in}}, a_{2,\text{in}}, a_{3,\text{in}}\right)^T$ and $v_{out} = \left(a_{1,\text{out}}, a_{2,\text{out}}, a_{3,\text{out}}\right)^T$ are the frequency dependant input and output amplitude vectors. H is the 3×3 Langevin matrix, $K = Diag\left[\sqrt{\gamma_{1,\text{ex}}}, \sqrt{\gamma_{2,\text{ex}}}, \sqrt{\gamma_{3,\text{ex}}}\right]$; is the diagonal matrix which describes the coupling to the environment and $M = (H - iI\omega)^{-1}$. From eq. (2.3) and eq. (2.5) we have,

$$M^T = U_\phi M U_\phi^\dagger \tag{2.6}$$

where the unitary matrix $U = Diag\left[e^{i\phi_1}, e^{i\phi_2}, e^{i\phi_3}\right]$ with ϕ_js being the phases of the pumps which drives the modes and we can assume, without loss of generality, that $\phi_1 + \phi_2 + \phi_3 = 0$. We can represent the matrix M as

$$M = \begin{bmatrix} \Delta_1 & g_{12} & g_{13} \\ g_{21} & \Delta_2 & g_{23} \\ g_{31} & g_{32} & \Delta_3 \end{bmatrix} \tag{2.7}$$

Hence our condition for a reciprocal system becomes $\phi_j - \phi_k = -2\delta_{jk} + n_{jk}\pi$; where δ_{jk} is the phase of the coupling coefficient. Graphically, the diagonal elements of M are the weights of the *self-loops* in the graph in fig. 2.2 and the off-diagonal elements, the couplings, are the weights of the directed branches. Within this representation, we sum the above reciprocity condition along every closed loop L, which

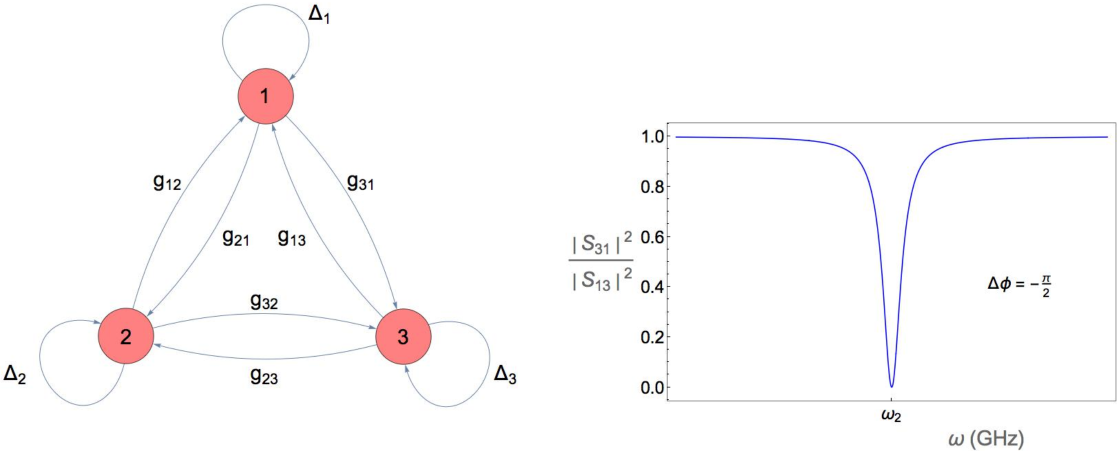

(a) *(b)*

Figure 2.2 – (a)Directed graph picture for the Langevin matrix of a 3 mode coupled system. The non-reciprocity condition in eq. (2.9) involves the interference between the paths g_{21}, g_{32} and g_{13} . (b) Ratio of off-diagonal scattering matrix elements for the Josephson Parametric Converter(JPC). We see that for optimal choice of pump phases. one can get directional scattering of EM modes. In the case of the JPC, each of the 3 modes can be made to interact with the other two modes in such a way so as to achieve non-reciprocal devices such as isolator and directional amplifier.

yields

$$\sum_{j,k\in \mathrm{L}} \delta_{jk} = n_{\mathrm{L}}\pi \tag{2.8}$$

where n_{L} is an integer. Hence, in order to realise a non-reciprocal system, eq. (2.8) must be violated. However, this only achieves phase non-reciprocity. In order to realise amplitude non-reciprocity between modes, say 1 and 2, we look at the ratio of off-diagonal scattering matrix elements of the modes coupled via frequency conversion ($g_{kj} = -g_{jk}$) . Hence, for maximum isolation ($\frac{S_{12}}{S_{21}} = 0$), we find that

$$\frac{g_{13}g_{32}}{2g_{21}^{*}} = \omega - \omega_3 + i\frac{\gamma_3}{2} \tag{2.9}$$

If the dissipation of mode 3; $\gamma_3 = 0$, then we see that the total phase on the LHS of eq. (2.9) (sum of phases in the loop $1 \to 3 : 3 \to 2 : 2 \to 1$) is zero. This does not violate eq. (2.9) and the 3^{rd} mode then acts as an internal lossless mode. The system behaves as a simple reciprocal two mode system. Hence we see that, in order to break reciprocal symmetry in a system, one needs a minimum of 3 dissipative modes, coupled to each other. In the above case, for zero detuning ($\omega = \omega_3$), the loop phase must be $\pi/2$ for perfect isolation. Physically, this condition for isolation can be visualised in the picture of interfering paths. The signal picks up different phases while traversing through the two coupling paths $1 \to 3 : 3 \to 2$ and $1 \to 2$) resulting in interference (fig. 2.2). By tuning the phase difference, one can induce destructive interference between the two pathways, thereby achieving directional coupling in the system.

Using similar analysis as above, one can induce non-reciprocal interaction between modes 2 & 3 and also 3 & 1, realising a frequency circulator. The obvious advantage in this scheme is that reciprocal symmetry is being broken without the use of an external magnetic bias. In fact, the total phase difference in such a circulator scheme acts as an artificial gauge flux and plays the role of the magnetic field in a conventional circulator. This is one of the motivations to further investigate and experimentally realise such a system. Also, by inducing a parametric amplifier type interaction between the modes, instead of frequency conversion, such a system can also be operated as a directional amplifier. One can, in principle, generalise the above analysis for an N-mode system, as we will see in the next chapter.

2.3 Reconfigurable Non-Reciprocal Device

A non-reciprocal device, based on the above theoretical framework has been demonstrated using a Josephson Parametric Converter [27] , recently. This scheme utilises a ring of four Josephson junctions in a loop threaded by a magnetic flux close to a half-flux quantum (Josephson Parametric Converter (JPC)). This small magnetic bias sets up a trilinear three body interaction between the three orthogonal modes (a,b,c) of the system. By off-resonantly driving one mode with a cw tone of the appropriate frequency, it is possible to produce one of two kinds of two-body interactions between the other two modes. On driving mode, say c, at the difference frequency of the other two ($\omega_c^p = \omega_a - \omega_b$) , one can induce a frequency conversion (or beam-splitter) like Hamiltonian between modes a and b. By simultaneously driving the other two modes in the same fashion, all the three modes of the JPC can be coupled to each other via frequency conversion. Moreover, by controlling the three pump phases, an input signal at one of the modes can be set to interfere such that there is a preferred directionality in sequential frequency conversion. The interaction between modes look like

$$\begin{aligned} \hat{H}_a &= \hbar g_a \left(e^{i\phi_a} \hat{c}\hat{b}^\dagger + e^{-i\phi_a} \hat{c}^\dagger \hat{b} \right) \\ \hat{H}_b &= \hbar g_b \left(e^{i\phi_b} \hat{a}\hat{c}^\dagger + e^{-i\phi_b} \hat{a}^\dagger \hat{c} \right) \\ \hat{H}_c &= \hbar g_c \left(e^{i\phi_c} \hat{a}\hat{b}^\dagger + e^{-i\phi_c} \hat{a}^\dagger \hat{b} \right) \end{aligned} \tag{2.10}$$

where g and ϕ represents the pump powers and phases, with the subscripts denoting the pump. The total phase difference, given by $\Delta\phi = \phi_a + \phi_c - \phi_b$, controls the interference. Moreover, this $\Delta\phi$ can be absorbed into a single pump phase(*synthetic gauge*) keeping all the other pump phases to zero, without loss of generality, thereby reducing the system to one dimension in ϕ. This system can be solved(fig. 2.2(b)), using the Langevin treatment in the Fourier domain for the ratio of conversion coefficients $|S_{31}/S_{13}|^2$. For the above system, any one of the 3 modes can be taken as input while either of the other 2 modes can be the output. Hence, a frequency conversion circulator is realised. Conversely, any two modes can be set to interact via a gain process (parametric amplifier) by pumping one mode at the sum frequency of the other two.

2.4 Non-Reciprocity via Engineered Reservoir

Another approach, that was put forward in [5], is the notion of reservoir engineering. As studied in section 2.1, dissipation plays a key role in symmetry breaking and the idea behind this particular scheme is to engineer an interaction between the EM modes that is inherently dissipative. By suitably tuning a coherent interaction against this lossy one, the modes can be made to interact non-reciprocally. To illustrate this, consider a coupled 3 mode system as shown in fig. 2.3 (a) where EM modes 1 and 2 are interacting coherently through a J-coupling and dissipatively via mode 3. Let all the interactions be of *beam-splitter* type and hence the Hamiltonian(in the rotating frame) is given by

$$\hat{H} = J\hat{a}_1^\dagger \hat{a}_2 + \gamma \hat{a}_1 \hat{b}^\dagger + \gamma e^{-i\phi} \hat{a}_2 \hat{b}^\dagger + c.c. \tag{2.11}$$

where J and γ are the interaction rates between the modes. Assuming decay rates of κ_1, κ_2 and Γ for the three modes respectively, the equations of motion for the system are given by :

$$\dot{\hat{a}}_1 = -\frac{\kappa_1}{2}\hat{a}_1 - iJ\hat{a}_2 - i\gamma\hat{b} \tag{2.12}$$

$$\dot{\hat{a}}_2 = -\frac{\kappa_2}{2}\hat{a}_1 - iJ^*\hat{a}_1 - i\gamma e^{-i\phi}\hat{b} \tag{2.13}$$

$$\dot{\hat{b}} = -\frac{\Gamma}{2}\hat{a}_1 - i\gamma\hat{a}_1 - i\gamma e^{-i\phi}\hat{a}_2 \tag{2.14}$$

We assume no internal loss for the modes to keep the calculation simple. Eliminating the 3^{rd} mode by assuming a steady state, we can write the reduced coupled equations for $\hat{a}_1$ and $\hat{a}_2$

$$\dot{\hat{a}}_1 = -\left(\frac{\kappa_1}{2} + \beta\right)\hat{a}_1 - \left(iJ + \beta\right)\hat{a}_2 \tag{2.15}$$

$$\dot{\hat{a}}_2 = -\left(\frac{\kappa_2}{2} + \beta\right)\hat{a}_2 - \left(iJ^* + \beta\right)\hat{a}_1 \tag{2.16}$$

where we have made a gauge transformation, absorbing the phases into J and J* and $\beta = \frac{2\Gamma^2}{\gamma}$. From the above equations, we can clearly see that for the particular choice of $J = i\beta$, we can decouple $\hat{a}_2$ from $\hat{a}_1$, but not vice versa. This implies that mode 1 dynamics depends upon mode 2 but not the other way around, hence achieving non-reciprocity. The caveat in realising such a scheme is engineering a reservoir for the EM modes. In the context of optomechanics, the decay rates of the EM modes are much higher than that for the mechanical mode. Although, recently it was theoretically proposed that the mechanical mode could be engineered it into a cold, dissipative bath for an EM mode [2] . The key idea in this proposal is to utilise sideband cooling via another EM mode to tune the mechanical decay rate to achieve *Reverse Dissipation Regime* (RDR) (in contrast to *Normal Dissipation Regime* (NDR) where the decay rate of the mechanical mode is lower than that of EM mode).

Our ultimate aim, then, is to achieve RDR between EM mode($\hat{a}$ with decay rate κ_a) and mechanical mode($\hat{b}$ with decay rate Γ). Looking at the equations of motion in eqs. (1.18) and (1.19), we see that they are symmetric with respect to interchanging the EM and mechanical degrees of freedom (within noise inputs). Hence, this regime acts as a dual to the optomechanical phenomena in NDR. This is clearly seen in fig. 2.3(a) in which the response of an EM mode in RDR is shown. Conceptually, achieving RDR using a cooling mode($\hat{c}$ with decay rate κ_c) can be thought of as two independent processes where the mechanical oscillator is cooled by the auxiliary mode which is then seen by the primary mode as a cold, dissipative bath. Such a scheme brings the system to a hierarchy $\kappa_a << \Gamma_\mathrm{eff} << \kappa_c$, where Γ_eff is the engineered mechanical damping rate (hierarchy in the NDR was $\Gamma << \kappa_a << \kappa_c$).

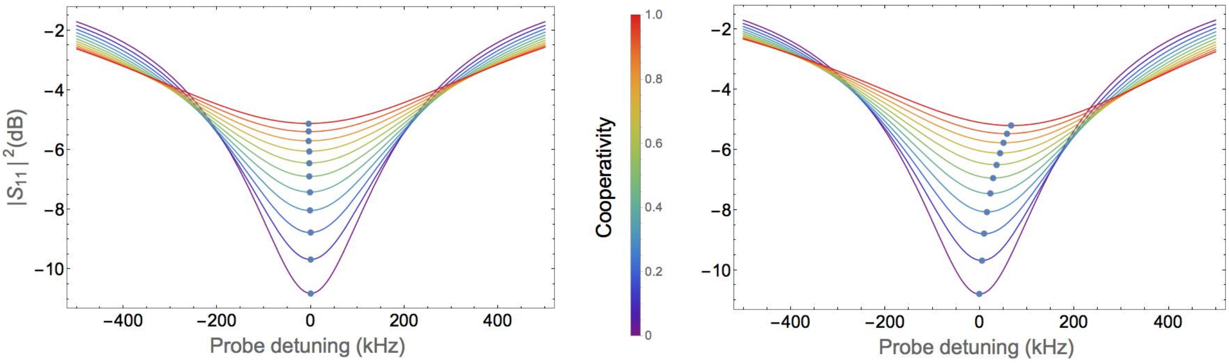

Figure 2.3 – (a)Linear response of an EM mode coupled to an ideal reservoir with increasing Cooperativity $\mathscr{C}$. As $\mathscr{C}$ is increased, the effective internal loss of the cavities are modified due to the optomechanical interaction, leading to shallow peak height [3] .(b) RDR achieved via sideband cooling using an auxiliary mode. We see a shift in the resonance frequency due to an optomechanical spring effect caused by the effective coupling between the two EM modes via the mechanics.

Having said this, the system we look at, with the interaction Hamiltonian

$$\hat{H}_{\text{int}} = g_1 \hat{a}^\dagger \hat{b} + g_2 \hat{c}^\dagger \hat{b} + c.c \tag{2.17}$$

does not perform exactly as expected (fig. 2.3(b). Even though the cooling mode($\hat{c}$) is, in principle, decoupled from the primary EM mode, there exists an effective coupling between them which is mediated by the mechanical oscillator. This coupling causes an *optomechanical spring effect* which shifts the resonance frequency of the first mode. That is to say, the interaction between the primary EM mode and the mechanical mode is affected by the presence of cooling mode in the form of a frequency shift, in addition to tuning the mechanical damping rate.

Recently, this scheme has been realized experimentally using microwave resonators and this thesis will follow the description and system parameters employed in [3] . In this work, a microwave resonator sustaining two eigenmodes, is coupled to a drum capacitor which acts as the mechanical element. The fundamental drum mode of the capacitor is coupled to both the microwave modes, of which one(*auxiliary mode*) is strongly over coupled compared to the other(*primary mode*). The Lorentzian feature, thus, of the auxiliary mode is engineered to be around 25 times wider as compared to the primary mode. Consequently, this mode is pumped on lower mechanical sideband (red sideband), to damp the mechanics. The system, thus achieves RDR with respect to the primary mode and the system is further investigated in this regime. Experimental results are consistent with the simulations in Fig. fig. 2.3(b) in the red detuned case. The system also achieves parametric amplification and instability when the primary mode is driven on the blue sideband.

3 Non-Reciprocity in OM Systems

In this chapter we investigate reciprocal symmetry breaking in systems where the couplings are mediated via mechanical oscillators. ie, all the modes present in the system are coupled via optomechanical interactions. For simplicity we will assume, for all the schemes discussed, the interaction between the EM and mechanical modes to be of frequency conversion (beam-splitter or hopping) type. Such an interaction can be achieved by pumping the modes at the lower sideband, with a detuning equal to the mechanical oscillator frequency. Utilising such an interaction, it is possible to realise isolators or even circulators from the schemes discussed below. On the other hand, by pumping the modes on the upper sideband with the same detuning, the modes will interact in a gain process (parametric amplifier) which can consequently lead some of the schemes to produce directional amplifiers.

3.1 The Simplest System

We start with the most basic system of two coupled electromagnetic modes and aim to achieve non-reciprocal interaction between the two. As mentioned, all the couplings are optomechanical and hence, clearly, we need two mechanical modes to complete the system. Hence, the simplest optomechanical coupled mode system required to break reciprocity between two EM modes is shown in Fig fig. 3.1.

The full Hamiltonian of the system containing 2 EM modes ($\hat{a}_1$, $\hat{a}_2$; frequency ω_1, ω_2) and 2 mechanical modes ($\hat{b}_1$, $\hat{b}_2$; frequency Ω_1, Ω_2) can be written as (in units of $\hbar$) :

$$\hat{H} = \omega_1 \hat{a}_1^\dagger \hat{a}_1 + \omega_2 \hat{a}_2^\dagger \hat{a}_2 + \Omega_1 \hat{b}_1^\dagger \hat{b}_1 + \Omega_2 \hat{b}_2^\dagger \hat{b}_2 + \hat{H}_{\text{int}} + \hat{H}_{\text{drive}} \tag{3.1}$$

where the interaction and drive Hamiltonians are given by :

$$\hat{H}_{\text{int}} = (\hat{b}_1 + \hat{b}_1^\dagger)\left[G_{11} \hat{a}_1^\dagger \hat{a}_1 + G_{21} \hat{a}_2^\dagger \hat{a}_2\right] + (\hat{b}_2 + \hat{b}_2^\dagger)\left[G_{12} \hat{a}_1^\dagger \hat{a}_1 + G_{22} \hat{a}_2^\dagger \hat{a}_2\right] \tag{3.2}$$

$$\begin{aligned} \hat{H}_{\text{drive}} = {} & \alpha_1 e^{-i\omega_{11} t} \hat{a}_1^\dagger + \alpha_1 e^{-i\omega_{12} t} \hat{a}_1^\dagger + \alpha_2 e^{-i\omega_{21} t} \hat{a}_2^\dagger + \alpha_2 e^{-i\omega_{22} t} \hat{a}_2^\dagger \\ & + \text{c.c.} \end{aligned} \tag{3.3}$$

Here $G_{ij}(\omega_{ij})$ represents the optomechanical coupling strength(pump frequency) between the i^{th} EM mode and j^{th} mechanical mode while α_i is the pump or carrier amplitude which drives the interaction

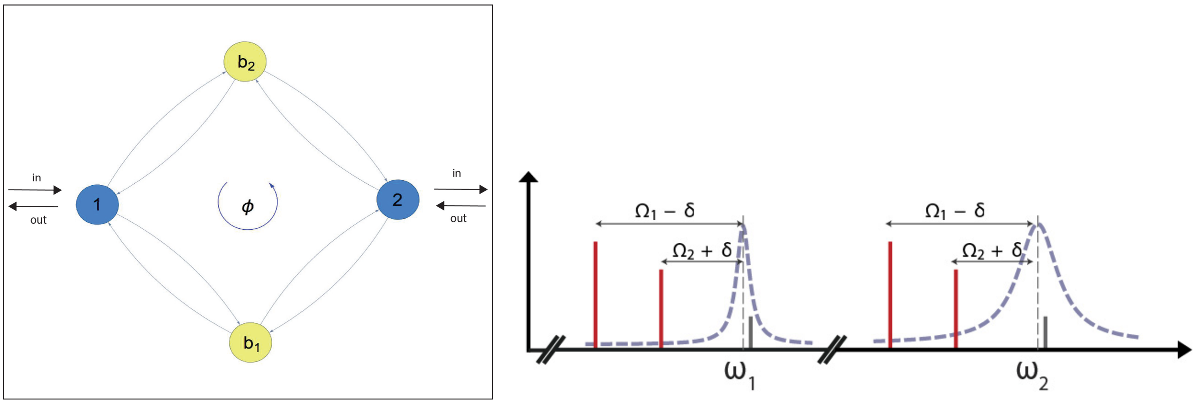

(a) (b)

Figure 3.1 – (a)Coupling scheme for the simplest pure optomechanical multimode non-reciprocal system. The blue disks represent the EM modes which are used as the "ports" in frequency space while the yellow disks depict the mechanical modes which mediate the coupling between the ports. The various pump phases in the system can be absorbed into one phase ϕ which can be tuned to get non-reciprocal interaction via interfering paths. (b) shows the frequency landscape depicting the positions of the cavities and the pumps used to set up the system.

between i^{th} EM mode and the mechanical modes $(i, j = 1,2)$. We move into an arbitrary rotating frame where all the modes are stationary and linearise the Hamiltonian by setting

$$\begin{aligned}
\hat{a}_1 &\to \alpha_1 e^{-i\omega_1 t}\left(\hat{a}_1 + e^{i\Delta_{11} t}\right) \\
\hat{a}_2 &\to \alpha_2 e^{-i\omega_2 \mathrm{t}}\left(\hat{a}_2 + e^{i\Delta_{22} t}\right) \\
\hat{b}_1 &\to \hat{b}_1 e^{i\Omega_1 t} \\
\hat{b}_2 &\to \hat{b}_2 e^{i\Omega_2 t}
\end{aligned} \tag{3.4}$$

and similarly for complex conjugate variables. Here the drive frequency is detuned from the cavity frequencies by $\omega_{ij} = \omega_i - \Delta_{ij}$ (where $i, j = 1,2$). Also, $\hat{a}_1^\dagger \hat{a} \approx \alpha_1 \hat{a}_1 e^{-i\Delta_{11} t} + \alpha_1^* \hat{a}_1^\dagger e^{i\Delta_{11} t}$. Therefore,

$$\begin{aligned}
\hat{H}_{\mathrm{lin}} = &\left(\hat{b}_1 e^{i\Omega_1 t} + \hat{b}_1^\dagger e^{-i\Omega_1 t}\right)\left[g_{11}\hat{a}_1 e^{-i\Delta_{11} t} + g_{21}\hat{a}_2 e^{-i\Delta_{21} t} + \mathrm{c.c.}\right] + \\
&\left(\hat{b}_2 e^{i\Omega_2 t} + \hat{b}_2^\dagger e^{-i\Omega_2 t}\right)\left[g_{12}\hat{a}_1 e^{-i\Delta_{1h} t} + g_{22}\hat{a}_2 e^{-i\Delta_{22} t} + \mathrm{c.c.}\right]
\end{aligned} \tag{3.5}$$

where $g_{ij} = G_{ij}|\alpha_i|^2$ is the pump power dependent coupling strength. Now, in order to induce frequency conversion interaction between each of the modes, the pumps are driven on the red(lower) sidebands of the EM modes. We set detunings, therefore, as

$$\begin{aligned}
\Delta_{11} &= -\Omega_1 - \delta & \qquad \Delta_{12} &= -\Omega_2 + \delta \\
\Delta_{21} &= -\Omega_1 - \delta & \qquad \Delta_{12} &= -\Omega_2 + \delta
\end{aligned}$$

We introduce δ to be the detuning from the mechanical sideband. Therefore, the pumps driving the interaction between $\hat{b}_1$ and the 2 EM modes is driven with a frequency slightly lower than the mechanical sideband. The pumps driving $\hat{b}_2$ however, are driven with a slightly larger frequency. The reasoning behind this particular choice of pump positions will be discussed later in this chapter. Now, in order to make the Hamiltonian time independent, we move to a new rotating frame $\hat{b}_1 \to \hat{b}_1 e^{-i\delta \mathrm{t}}$; $\hat{b}_2 \to \hat{b}_2 e^{i\delta \mathrm{t}}$.

Hence the Hamiltonian of the system in the Rotating Wave Approximation(RWA) is

$$\hat{H}_{\text{lin}} = -\delta \hat{b}_1^\dagger \hat{b}_1 + \delta \hat{b}_2^\dagger \hat{b}_2 + e^{-i\phi} g_{11} \hat{a}_1 \hat{b}_1^\dagger + g_{21} \hat{a}_2 \hat{b}_1^\dagger + g_{12} \hat{a}_1 \hat{b}_2^\dagger + g_{22} \hat{a}_2 \hat{b}_2^\dagger + \text{c.c.} \tag{3.6}$$

In this frame, both the EM modes have zero frequency and the mechanical modes are detuned from then by ±δ. Without loss of generality, all couplings are taken to be real except for the one between $\hat{a}_1$ and $\hat{b}_1$ that has a complex phase ϕ. It introduced here can be thought of as the relative phase of the pump with respect to the other 3(which are coherent). This is valid since it is the relative phase difference between the pumps that is picked up by the signal at the output. Moreover, in microwave experiments, all the pumps are phase locked with respect to a master clock(tone) and the phase difference is measured in reference to this clock. We now write the Langevin matrix for the system

$$M = \begin{bmatrix} -\frac{\kappa_1}{2} & 0 & -ig_{11}e^{-i\phi} & -ig_{12} \\ 0 & -\frac{\kappa_2}{2} & -ig_{21} & -ig_{22} \\ -ig_{11}e^{i\phi} & -ig_{21} & i\delta - \frac{\Gamma_1}{2} & 0 \\ -ig_{12} & -ig_{22} & 0 & -i\delta - \frac{\Gamma_2}{2} \end{bmatrix} \tag{3.7}$$

which satisfies the differential equation $\dot{v} = Mv$, where $v = \left[\hat{a}_1, \hat{a}_2, \hat{b}_1, \hat{b}_2\right]^T$. From here, one can solve to get the scattering matrix (S) in the frequency domain using the input-output relations. We now investigate this system further to realise an ideal isolator. Assuming the ports are the frequencies of the EM modes, we now look for the condition where $S_{12} = 0$. i.e., a signal input at port 2 is not transmitted to port 1. To simplify this analysis, the two mechanical modes are assumed to have identical decay rates ($\Gamma_1 = \Gamma_2 = \Gamma$). We find that for Δ_p, δ and ϕ satisfying

$$\frac{\Gamma}{2\delta} = i\frac{\Delta_\text{p}}{\delta} - \tan\left[\frac{\phi}{2}\right] \tag{3.8}$$

transmission from ports 2 to 1 is suppressed. Here Δ_p is the probe detuning from the cavity resonance ($\omega = 0$ in rotating frame). Since the left hand side of the equation is a real number, we arrive at conditions for Δ_p and Γ_1 revealing that we can completely suppress transmission from 2 → 1 on resonance. A two port ideal isolator has the scattering matrix

Now we use eq. (3.8) to find the condition where $|S_{21}|^2$ is maximized. We operate under the assumption that all the pumps are being driven with the same cooperativities $\mathscr{C}$. We derive the optimum cooperativity $\mathscr{C}_\text{opt}$, for maximum transmission from 1 → 2 as a function of ϕ (and hence δ) as

$$\mathscr{C}_\text{opt} = \frac{1}{1 - \cos\phi} \tag{3.9}$$

The maximum conversion varies with the ϕ as $|S_{21}|^2_\text{max} = \cos^2\frac{\phi}{2}$. For optimal choices of δ and $\mathscr{C}$, the scattering matrix of this system asymptotically approaches to that of an ideal isolator (fig. 3.2 a). The above analysis was performed for a system without any internal losses. While the conditions for maximum isolation does not change when the effect of the losses inside the cavities are taken into account, the maximum isolation is now limited by the product of coupling efficiencies for the two cavity modes $\eta_1\eta_2$ (fig. 3.2 b).

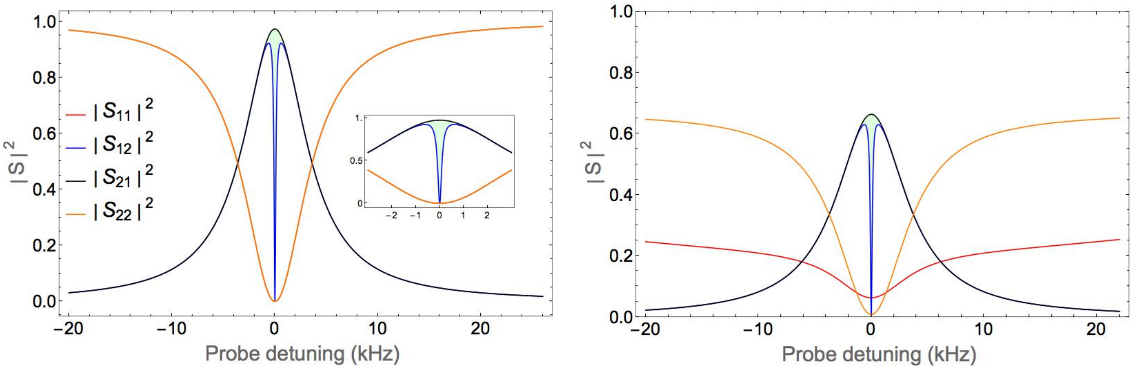

(a) *(b)*

Figure 3.2 – Scattering matrix elements for transmission and reflection from the ports vs probe detuning from the resonance ($\omega = 0$) for system parameters and $\delta = 30\,\text{Hz}$. (a) shows the case when there is no internal loss associated with the cavity photons. The scattering matrix is close to that of an ideal isolator. Lightly green shaded region shows the difference in the off diagonal elements. Inset shows the graph zoomed around the resonance to better gauge the bandwidth of isolation($\approx \Gamma$). From the equations for maximum transmission, it is clear that for ideal isolation, the pump powers would have to be increased to extremely high values. (b) depicts the scattering matrix elements for cavity modes with internal loss. The maximum transmission is now limited by the product of coupling efficiencies of the individual cavity modes.

The extend of non-reciprocity can be measured by the ratio of off-diagonal scattering matrix elements :

$$|\mathscr{R}|^2 = \frac{|S_{12}|^2}{|S_{21}|^2} \tag{3.10}$$

Isolation yields $\mathscr{R} = 0$ or ∞ (isolation in the reverse direction) and in general, this ratio is a function of δ and ϕ (fig. 3.4). In the case when $\delta = 0$, eq. (3.8) does not have a solution (since $\Gamma_g \neq 0$) and hence the system ceases to be non-reciprocal, on resonance. The introduction of antisymmetric detunings ($+\delta$ and $-\delta$) from the two mechanical sidebands, is therefore used to unhinge the system from this highly symmetric configuration. Shifting the pumps to the same side would not break the symmetry, as the modes can be brought back to resonance by moving to an appropriate rotating frame. Having stated this, non-reciprocity may well be exhibited by the system due to higher order terms emerging when the mechanical decay rates (Γ) are different for the two oscillators (and $\phi \to -\pi/2$). But this form of superficial non-reciprocity, as shown in fig. 3.4, is severely bounded in isolation. The reason for suppression of first order non-reciprocity is due to the high level of symmetry the system possesses where the Lorentzian responses for the modes are aligned on resonance.

The origin of the non-reciprocity in this system can be understood from eq. (3.10). Expanding we get :

$$\mathscr{R} = \frac{e^{-i\phi} g_{11} g_{21} \chi_1(\omega) + g_{12} g_{22} \chi_2(\omega)}{e^{+i\phi} g_{11} g_{21} \chi_1(\omega) + g_{12} g_{22} \chi_2(\omega)} \tag{3.11}$$

where $\chi_1^{-1}(\omega) = \Gamma_1/2 - i(\delta + \omega)$ and $\chi_2^{-1}(\omega) = \Gamma_2/2 + i(\delta - \omega)$ are the mechanical susceptibilities. The individual terms represent the frequency conversion Lorentzian features between the two paths ($1 \to 2$ and $2 \to 1$). From one direction to the other, the phase ϕ of the coherent coupling is conjugated, while the complex phase associated with the response of the mechanical modes stays constant. This can be interpreted as two differing phase pick ups for the two pathways leading to constructive or destructive

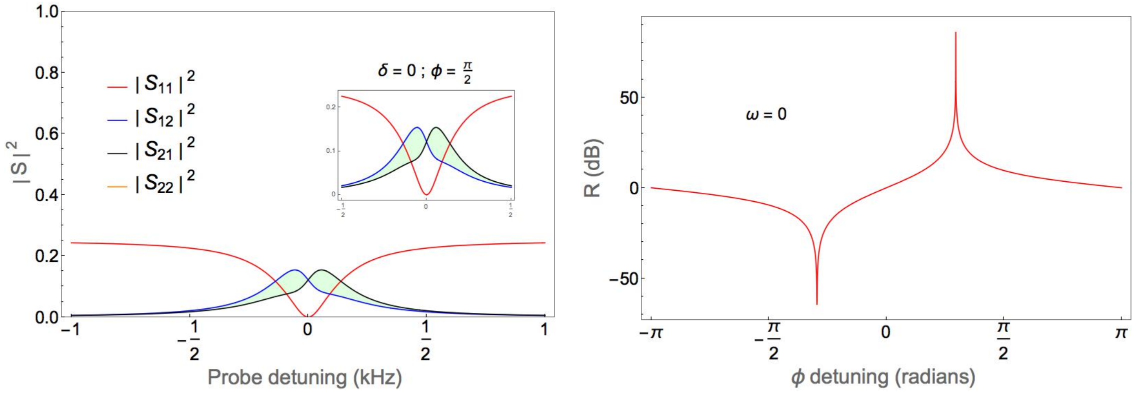

(a) *(b)*

Figure 3.3 – (a) Scattering matrix elements for transmission and reflection from the ports vs probe detuning from the resonance ($\omega = 0$) for system parameters, $\delta = 0$ and $\phi = \pi/2$. We see that due to the high symmetry that the system possesses, there is no non-reciprocity on resonance. The superficial non-reciprocity (green shaded portion) is due to the difference in the decay rates of the two mechanical modes. The optimum non-reciprocity thus achieved is severely limited, as shown. (b) depicts the ratio of off-diagonal scattering matrix elements for cavity modes with internal loss on resonance. The isolation condition is periodic in phase space, as shown.

interference, which is determined by the phase relation eq. (3.7). The Lorentzians for the two pathways interfere creating a small window of non-reciprocity. This non-reciprocal bandwidth scales as the bare decay rate (Γ) of the mechanical modes. Here we can clearly see the vital role dissipation plays in non-reciprocity.

3.1.1 Effective Decay Rates Matched

In practice though, the bare decay rates of the two mechanical modes will not be identical and due to this, the conditions for maximum isolation will be affected. Additionally, since there is an obvious disruption in the system symmetry, the resonance frequency at which the interference occurs, is expected to shift . To obtain the new constraints on δ and ϕ, we take two cases. First wee assume that both the mechanics are driven with high pump powers and that the effective decay rate $\Gamma_{i,\text{eff}} = 2\mathscr{C}\Gamma_i$ where $\mathscr{C}$ is the cooperativity and $i = 1,2$. Now we assume both the effective decay rates to be equal to Γ_{eff}. The constraints are then,

$$\frac{\Gamma_+}{2\delta} = -\tan\left[\frac{\phi}{2}\right] \tag{3.12}$$

while the new resonance frequency is at

$$\Delta_\text{p} = \frac{\Gamma_+\Gamma_-}{4\delta} \tag{3.13}$$

where $\Gamma_\pm = \frac{1}{2}(\Gamma_1 \pm \Gamma_2)$. Now we try to find the optimum value of Γ_{eff} that maximizes $|S_{21}|^2$. Since $\Gamma_- < \Gamma_+ << \delta << \Gamma_{\text{eff}}$, we taylor expand the solution around $\Gamma_- = 0$ and obtain

$$\Gamma_{\text{eff}} \approx \frac{2\Gamma_+}{1-\cos\phi}\left(1 + \frac{2\Delta_\text{p}^2}{\Gamma_+^2}\right) \tag{3.14}$$

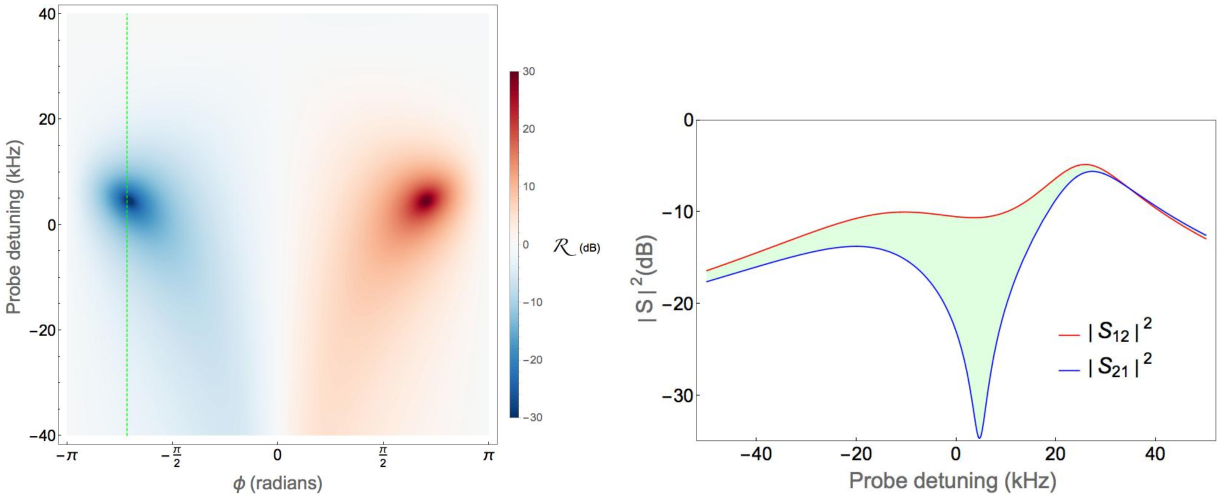

(a) *(b)*

Figure 3.4 – (a) Contour plot of R vs $\{\phi, \omega\}$ for the asymmetric case, $(\Gamma_1 \neq \Gamma_2)$ using system parameters given in table A.1 with the changes $\Gamma_1 = 2\pi\,6\,\text{kHz}$, $\Gamma_2 = 2\pi\,30\,\text{kHz}$, $\delta = 2\pi\,8\,\text{kHz}$. (The changes are made in order to fit to the experimental results [1]) (b) shows a vertical cut of the contour plot at $\phi = -2.3\,\text{rad}$.

For $\Gamma_- = 0$, we have $\omega = 0$ and $\Gamma_{\text{eff}} \to \Gamma^0_{\text{eff}}$. In the expression for $|S_{21}|^2$, the lowest order of Γ_- is 2, similar to the above equation involving Γ_{eff}. Therefore, the above correction will manifest in $|S_{21}|^2$ only in higher orders and can safely be neglected. That is,

$$\Gamma_{\text{eff}} \approx \Gamma^0_{\text{eff}} = \frac{2\Gamma_+}{1-\cos\phi} \tag{3.15}$$

Maximum value of $|S_{21}|^2$ also has a correction term because of non zero Γ_- and is given by

$$|S_{21}|^2_{\max} \approx \left(1 + \frac{2\Delta_{\text{p}}^2}{\Gamma_+^2}\right)\cos^2\frac{\phi}{2} \tag{3.16}$$

This scheme has been experimentally realized and briefly discussed in section (4.1).

3.1.2 Cooperativities Matched

Here, we match the cooperativities ($\mathscr{C}$) of the pumps driving the mechanics, instead of Γ_{eff}. In this case, the phase relation stays the same as eq. (3.10) but the resonance frequency shifts to a value given by

$$\Delta_{\text{p}} = -\delta\,\frac{\Gamma_-}{\Gamma_+} \tag{3.17}$$

Maximizing $|S_{21}|^2$ again, we get optimum cooperativity

$$\mathscr{C}_{\text{opt}} \approx \frac{1}{1-\cos\phi}\left[1 + \Delta_{\text{p}}^2\left(\frac{1}{\kappa_1^2} + \frac{1}{\kappa_2^2}\right)\right] \tag{3.18}$$

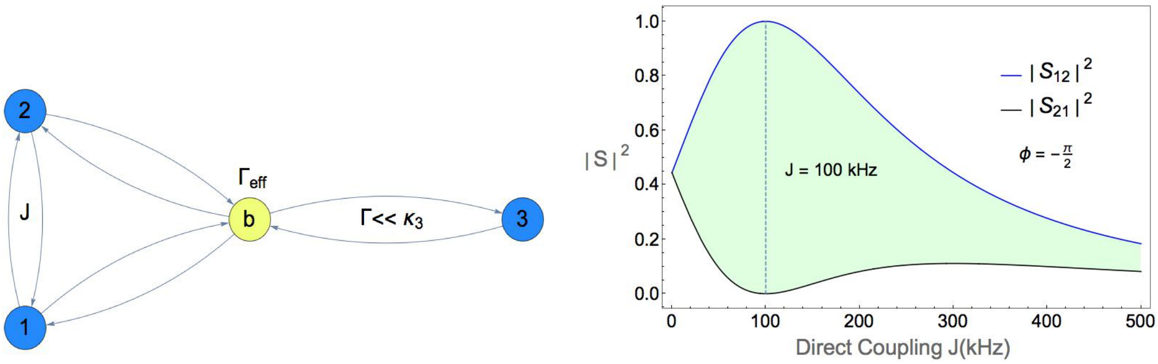

(a) *(b)*

Figure 3.5 – (a) Depiction of the coupling scheme between EM and mechanical modes. Blue disks represents EM modes and the yellow disk, the mechanical oscillator. EM modes 1 and 2 are coupled coherently via J-coupling and through a mechanical oscillator. (b) Optimal value of direct coupling for ideal isolation. Here we see that for J = 100 kHz, R = 0.

and maximum transmission

$$|S_{21}|^2_{\max} \approx \left[1 - \Delta_p^2\left(\frac{1}{\kappa_1^2}+\frac{1}{\kappa_2^2}\right)\right]\cos^2\frac{\phi}{2} \tag{3.19}$$

up to second order in Γ_- . As compared to the symmetric case (section 3.1.1), the corrections that appear when the bare decay rates of the mechanics are different ($\Gamma_- \neq 0$), are very small and the constraints seem to stay roughly the same. Also, the factor in eq. (3.19) containing the decay rates of the EM modes, decreases the maximum transmission as compared to eq. (3.16). Also, it is much easier to implement and visualize the effective decay rates than the cooperativities, in experiment.

As mentioned previously, the bandwidth of non-reciprocity is of the order of Γ, the decay rate of the mechanical modes and not the effective decay rate Γ_{eff}. Hence to obtain a wider feature, we employ cooling of the mechanics via another EM mode, which is described in detail in the next section.

3.2 4-Mode System using Engineered Reservoir

Here we discuss a system which involves balancing direct, coherent coupling between two microwave modes with a dissipative interaction, which is optomechanical in nature. The direct coupling can be achieved via any arbitrary method, say for example, using kinetic inductance in microwave circuit optomechanics(section 4.2). The full system Hamiltonian in the RWA can be written, from the coupling scheme fig. 3.5 (a) as

$$\begin{aligned}\hat{H}_{lin} = g_1\left(e^{i\phi}\hat{a}_1^\dagger\hat{b}+e^{-i\phi}\hat{b}^\dagger\hat{a}_1\right)+g_2\left(\hat{a}_2^\dagger\hat{b}+\hat{b}^\dagger\hat{a}_2\right)+g_3\left(\hat{a}_3^\dagger\hat{b}+\hat{b}^\dagger\hat{a}_3\right)\\ +J\left(\hat{a}_1^\dagger\hat{a}_2+\hat{a}_2^\dagger\hat{a}_1\right)\end{aligned} \tag{3.20}$$

where g_i is the determines the optomechanical coupling strengths for each of the 3 modes, J is the strength of direct coupling and ϕ is the phase of the pump. In the above system, the pumps are placed in such a way so that all the couplings are beam splitter type. Solving the Langevin system using the

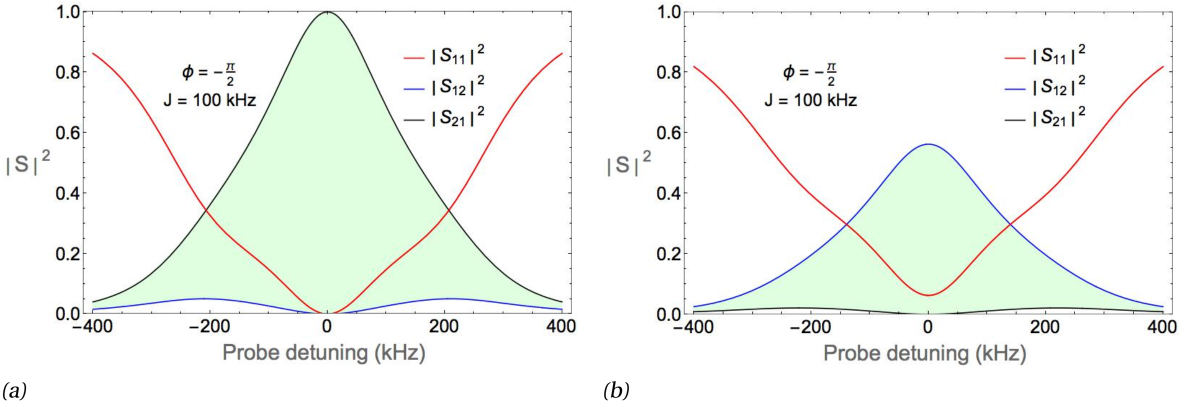

(a) (b)

Figure 3.6 – (a) Scattering matrix elements vs probe detuning at optimal choice of direct coupling and system parameters. The system in question is 2 EM modes coupled together coherently and dissipatively. The dissipative coupling is simulated by a mechanical mode with decay rate larger than that of the EM modes. Also, all the modes are assumed to have no internal losses. On resonance, the scattering matrix reduces to that of an ideal isolator. (b) Scattering matrix elements for a system of 2 EM modes coupled coherently and dissipatively. In this system, the dissipative coupling is provided by a mechanical oscillator which is sideband cooled using an additional EM mode. Due to this cooling, the effective decay rate of the mechanics (Γ_{eff}) is larger than the decay rates of the EM modes. To achieve maximum isolation, higher pump powers had to be used. Also, the isolation is limited by the coupling coefficients due to the finite internal losses associated with the cavities. In both the figures, the green shaded portion shows the extend of non-reciprocity. One can also clearly see the much larger bandwidth, as compared to the previous scheme discussed in section 3.1.

input-output relation in the Fourier space, we look at the response of the system. First we assume that the mechanical mode has an effective decay rate of $\Gamma = 500\,\text{kHz}$ and that it is decoupled from the 3rd EM mode. This is similar to the discussion in section 2.3 where the mechanical mode was considered to be an ideal reservoir with a decay rate much larger than the EM modes. Now we tune the direct coupling between the two electromagnetic modes in order to achieve perfect isolation ($\mathscr{R} = 0$) (fig. 3.5 (b)). The scattering matrix elements are shown in fig. 3.6 (a). It is evident from the response that the bandwidth of non-reciprocity is much larger than what is achievable using the previous scheme.

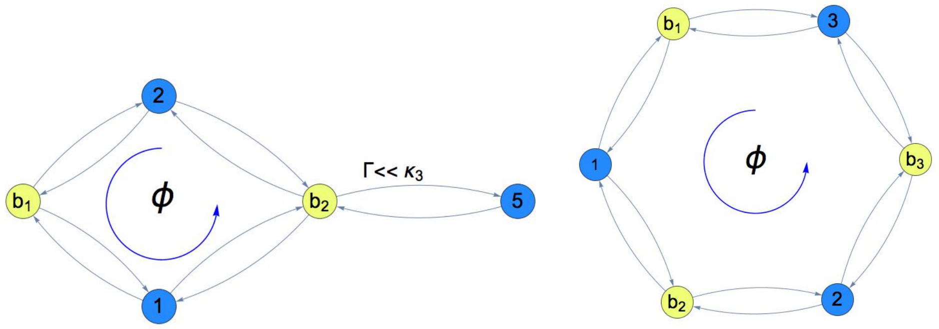

(a) *(b)*

Figure 3.7 – (a) Coupling scheme which extends the J-coupling scheme discussed in section 3.2. Both the interactions are mediated by mechanics. In principle, mode 5 can be coupled to $\hat{b}_1$ to cool it, as well. This would be an extension to the diamond scheme to increase the bandwidth of non-reciprocity(b) Scattering matrix elements for a system of 2 EM modes coupled coherently and dissipatively. (b) A 6-mode optomechanical frequency circulator that can, in theory, mimic the device fabricated using Josephson junction, mentioned in section 2.2

Extending this study, schemes with higher number of modes can also, in principle, show non-reciprocal behavior Replacing the J coupling in the above scheme with an optomechanical interaction can provide similar results, with the caveat that both the "coherent" and "dissipative" interactions have internal dissipation due to the mechanics. An extension to this scheme would be to use the cooling mode (mode 3) in the above description to cool both the mechanical modes, thereby realizing a more robust version of the scheme discussed in section 3.1 where the bandwidth can be increased by reservoir engineering. Finally, it might also be possible to realise a 6 mode system with alternating EM and mechanical modes to realise a purely optomechanical frequency circulator (fig. 3.7).

4 Non-Reciprocity Implementation

In this chapter we show the implementation of two schemes for non-reciprocity discussed in the previous chapter.

4.1 The Simplest System : 4 Modes

In order to realise such a scheme, we employ the same microwave cavity optomechanical system discussed in section 2.4, in which two microwave modes are coupled to the same mechanical oscillator. The two mechanical modes which mediate couplings between the microwave modes are two harmonic drum modes of the capacitor [1] . The scheme followed here is the same as studied in section 3.1.1. A maximum isolation of 20 dB in each direction is demonstrated using this system. Also, the experimental contour plot of the ratio of off-diagonal scattering matrix elements agrees well with the theoretical one shown in fig. 3.4.

This study provides the first insight into magnetic free non-reciprocity using purely optomechanical coupling. The further objectives would be to increase the bandwidth of non-reciprocity using a cooling tone coupled to both the mechanical oscillators.

4.2 4-Mode Reverse Dissipation Regime Scheme

Here we discuss the details of the circuit that was designed in order to realise the scheme studied in section (3.2). As discussed previously, this particular scheme requires 3 microwave modes coupled to the same mechanical oscillator. Out of these, 2 microwave modes will be coupled coherently while the third mode will be used to sideband cool the mechanical oscillator to realise a cold dissipative bath. Hence there exist a hierarchy of decay rates (κ_{ex}) for the microwave modes.

4.2.1 Constraints in Circuit Design

Due to device limitations and the uniqueness of the scheme, design of the circuit (modes) was heavily constrained.

- The optimum working range of the devices used in the experiment was approximately

4 - 8 GHz. That is, the three designed modes would have to lie in this particular range. This imposes constraints on the inductors and capacitors used.

- Since 2 microwave modes are coherently coupled together in, say, frequency conversion Hamiltonian, it would facilitate the interaction if the modes were closely spaced in frequencies. Hence the desirable arrangement of modes in frequency landscape would be 2 closely spaced modes and a third mode separated relatively farther in frequency, in the range of 4-8 GHz.
- The size of the circuit was of the order of hundreds of microns and would be implemented on a chip. Hence, the challenge was to design a compact, near lumped-element circuit. A larger circuit with many components would not only be difficult to implement, but also could suffer from parasitic capacitances due to its distributed nature, which can produce results deviating appreciably from theoretical analysis.
- The scheme relies on achieving RDR for 2 coupled microwave modes with respect to a mechanical oscillator. For this, a third mode will be used to cool the mechanics. Hence the hierarchy of external decay rates for the modes are given by $\kappa_{1,\text{ex}} \approx \kappa_{2,\text{ex}} >> \kappa_{3,\text{ex}}$. The bare mechanical decay rate Γ_m is usually much lower than the EM rates. But, due to sideband cooling, this effective damping rate $\Gamma_{\text{eff}} >> \kappa_{1,\text{ex}} \approx \kappa_{2,\text{ex}}$, hence achieving RDR.

The above constraints elevate the complexity of the problem immensely and realising such a scheme meant spending a considerable time of this thesis in circuit simulations using Sonnet EM Simulator. The starting point of the design was the 2 mode microwave circuit used to achieve RDR. By consequently adding elements and morphing the topology of the circuit, we were able to arrive at a nearly ideal circuit that satisfies all of the constraints listed above fig. 4.1.

4.2.2 Circuit Details

The circuit itself consists of 6 meander inductors, an interdigitated capacitor and two equal parallel plate capacitors. In the actual experiment, the parallel plate capacitors will be replaced by a single split-plate drum capacitor [28] which will act as the mechanical element. Due to the split plate arrangement of the drum, each arm connecting it will in effect see half of its total capacitance. This strategy is used in order to couple all the available modes to the common mechanical oscillator, as required by the coupling scheme. The proposed position of the mechanical element(drum capacitor) is clear from fig. 4.2. The response of the circuit in transmission (from port 2 to 1) is shown from fig. 4.3 where it is evident that the mode spacing requirements have been realised. The simulation results for the flow of currents in the three modes are depicted in creffig:4.2.4. Again, the idea is to use the mode at 4.5 GHz to engineer the decay rate of the mechanics using sideband cooling. This reservoir will then be used to couple the two modes around 7.5 GHz dissipatively. Such a dissipative interaction, along with a coherent(direct) coupling realised by kinetic inductance, is hoped to execute non-reciprocal behaviour discussed in section 3.2.

A crucial factor to estimate is the coupling of the modes to the mechanics. Since Sonnet is a pure EM simulator which does not allow one to do mechanical simulations, the optomechanical coupling rate(g_0) for the circuit modes was calculated using some assumptions. The mechanical motion causes a change in the capacitor plate separation, changing the capacitance. Due to this change, the frequency

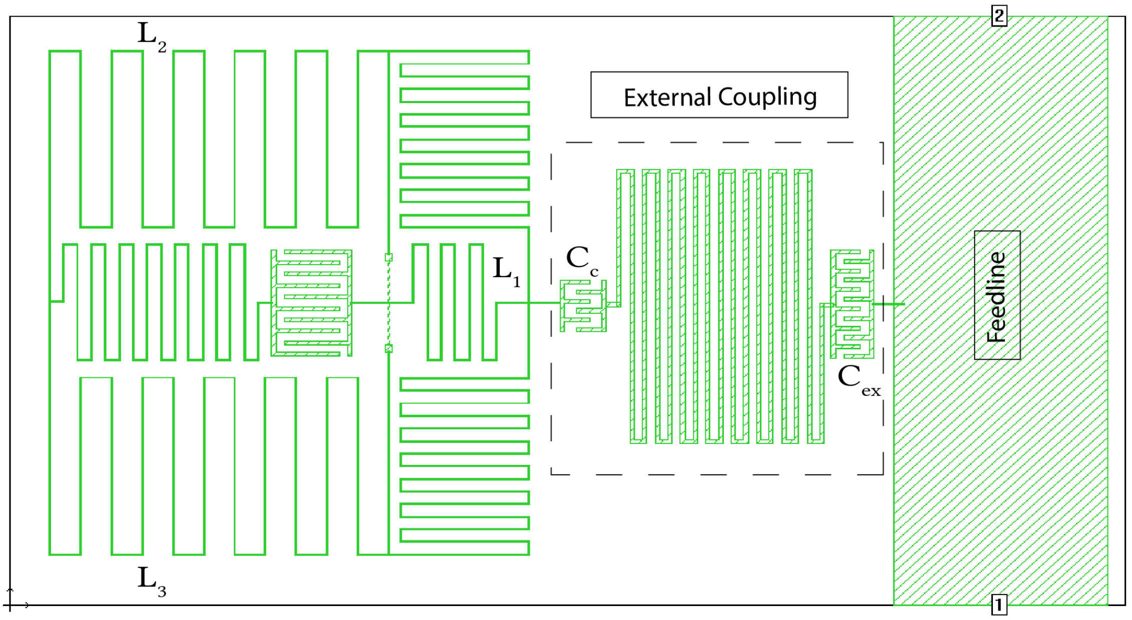

Figure 4.1 – The finalised circuit design proposed for Non-Reciprocity via engineered reservoir. The simulations were done using Sonnet, with superconducting Aluminium on top of a Sapphire substrate. The simulation box measure roughly 2.7 × 1.5 mm^2 while the circuit itself is about 1.2 × 1.3 mm^2

of the modes shift and this is measured by g_0. In the simplified optomechanical system shown in fig. 4.2, the mechanical motion occurs in the z-plane (the plane of the via). Hence, in order to gauge g_0, the distance between the two layers are varied in accordance with parameters observed in previous experiments(fig. 4.5). We assume that for a drum capacitor with plate separation 50 nm, the mechanical motion is of the order of 10 nm, which is around 7 orders of magnitude greater than the zero point fluctuations (section 1.7). The optomechanical coupling rates thus calculated are given in table 4.1

Mode (GHz)	Δf(GHz)	$\frac{g_0}{2\pi}$ (Hz)
4.595	0.104	52
7.419	0.304	152
7.516	0.25	125

Table 4.1 – Estimation of optomechanical coupling strength g_0 for the observed eigenmodes. The mechanical motion was emulated by changing the distance between the two layers containing the capacitor plates which then produces a frequency shift, Δf. The values estimated promise a fairly good coupling strength as compared to those experimentally observed.

These coupling rates are higher than the actual rates observed in other setups of similar fashion and hence indicates that all the modes are coupled well to the mechanics.

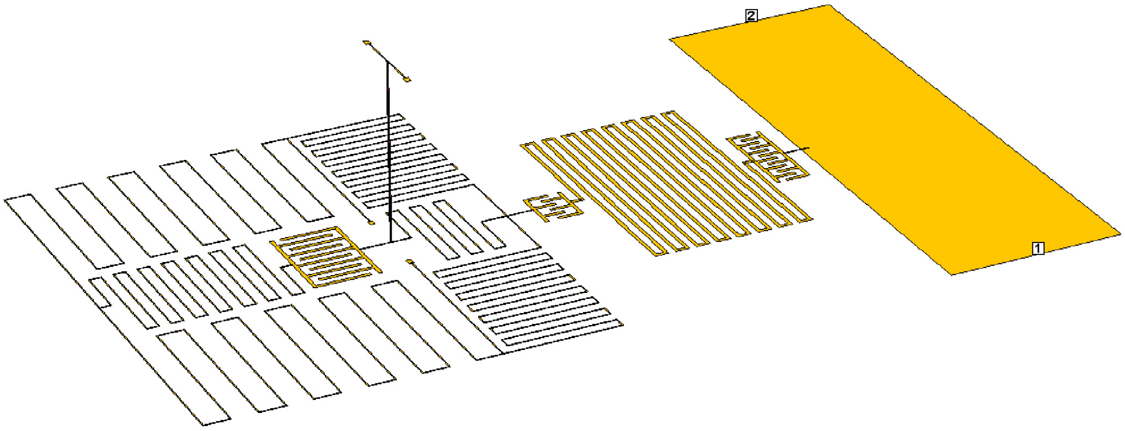

Figure 4.2 – 3D view of the finalised circuit design. The 2 parallel plate capacitors (connected to the bottom layer using a lossless via) mimic the effective capacitances seen by the horizontal arms when the mechanical element is placed in a split plate arrangement. In the fabricated circuit, the top plate of the drum capacitor will replace the connected top surfaces of the two parallel plates. Simulations were done with a plate separation of 50 nm, the typical distance between the plates of a drum capacitor.

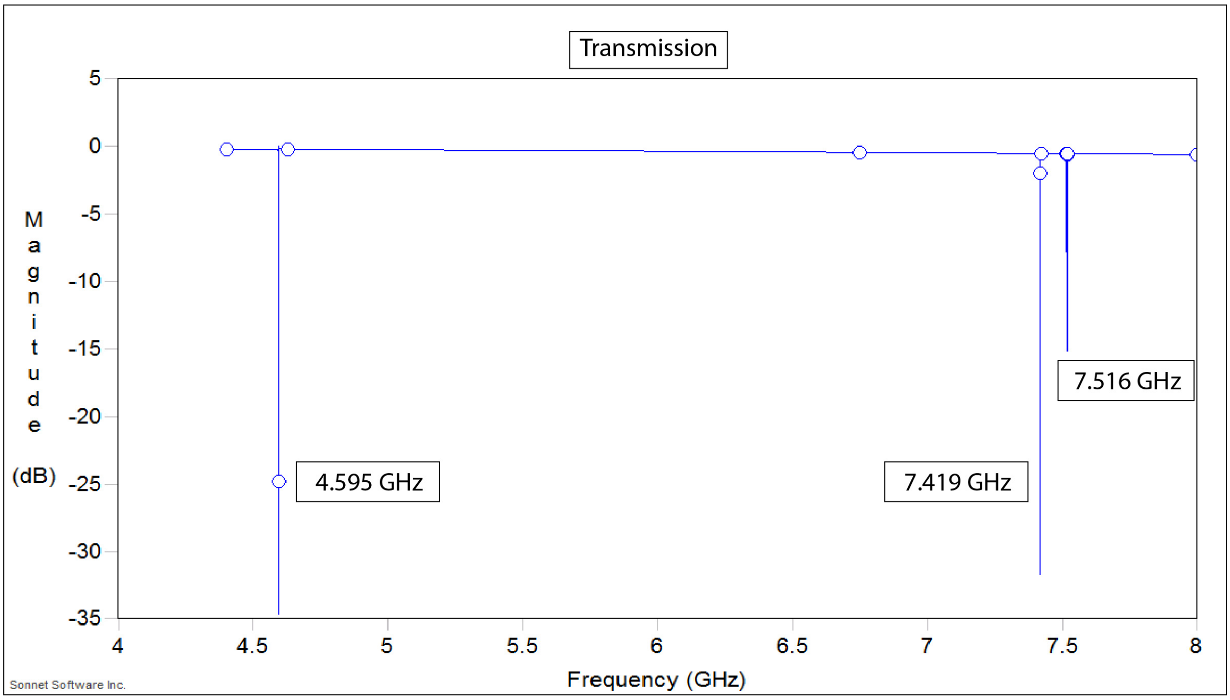

Figure 4.3 – Response of the circuit in transmission (port 1 → port 2) showing clearly the presence of 3 modes. The modes are spaced as desired, in order to optimize the implementation of this particular coupling scheme. (Sonnet simulations include negligible internal losses and hence the resonance peaks can be arbitrarily deep.)

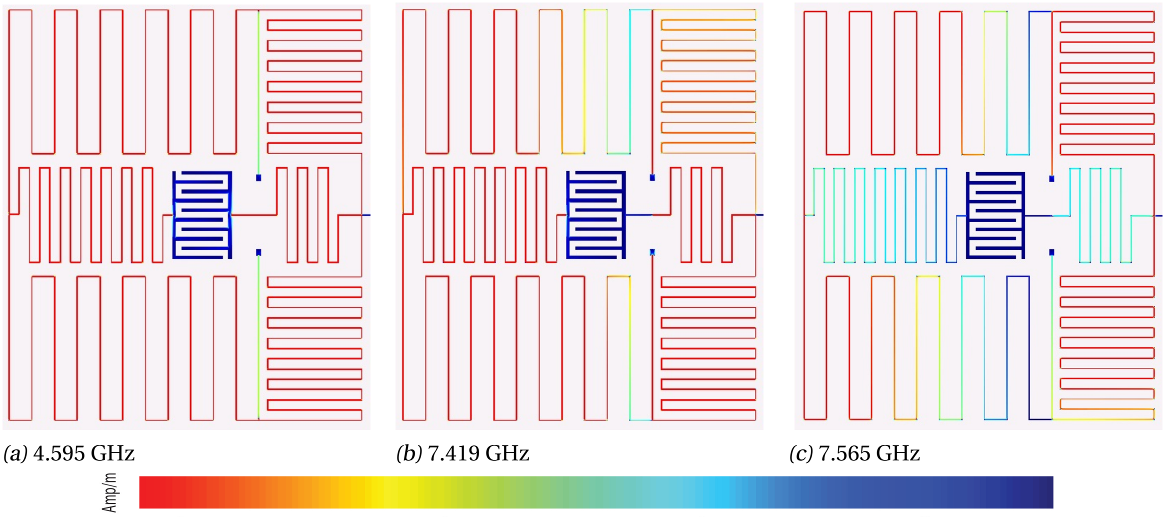
(a) 4.595 GHz (b) 7.419 GHz (c) 7.565 GHz

Figure 4.4 – Simulated results of the currents in each modes. The color bar represents the magnitude of current, increasing from blue to red, in the circuit. The first mode(a) has a strong current in the central horizontal arm with a weak current in the vertical one. (b) The second mode has a stronger current in the vertical arm with very little current in the central region connecting the interdigitated capacitor to the small inductor. (c) Mode 3 has current circulating only in the outer arms and the central vertical line, with little current in the horizontal one.

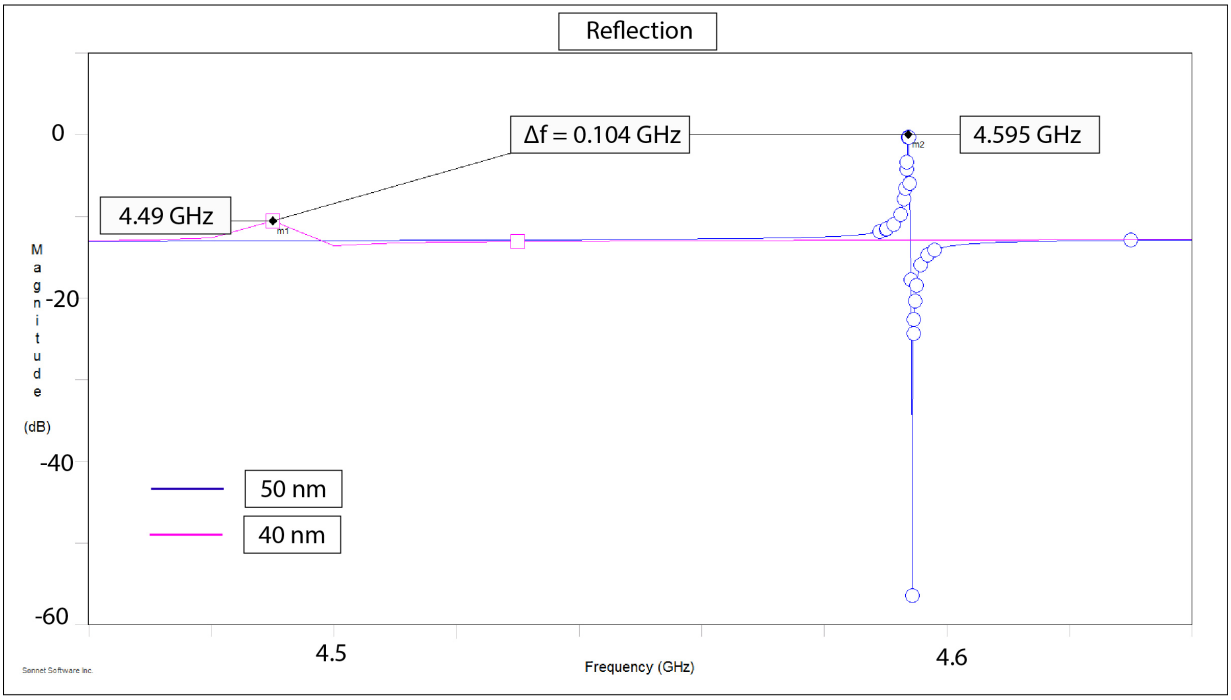

Figure 4.5 – Simulation results for the estimation of g_0 for the 4.6 GHz mode in reflection. The spacing between the layers containing the circuit and the top plate of the parallel-plate capacitor(in place of the mechanical element) is decreased from 50 nm to 40 nm, which roughly corresponds to the motion of the top plate of the drum capacitor in previous experiments. The red curve has fewer points since we were only interested in the position of the resonance and not the actual Lorentzian feature. Similarly g_0 is calculated for the other 2 modes.

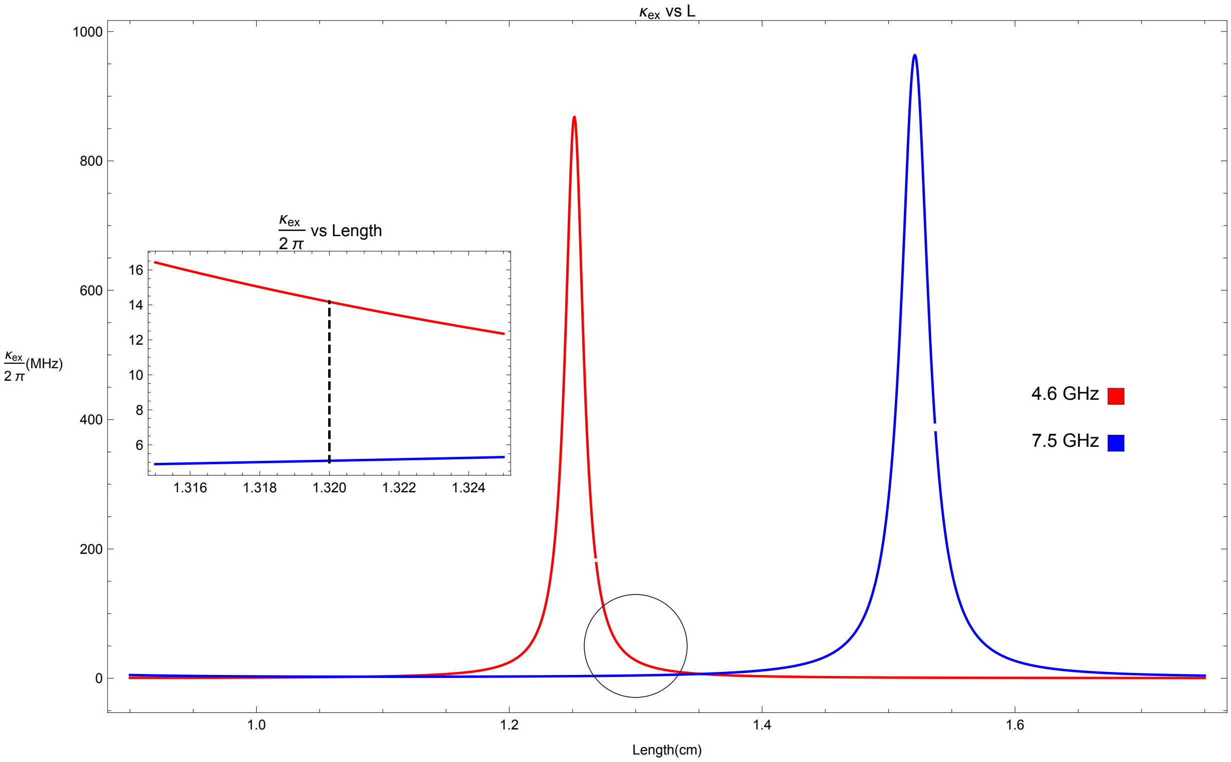

Figure 4.6 – The length of the impedance transformer is selected ($L = 1.32$ cm ;black dashed line in the inset ; zoomed around the circled portion) in order to get higher κ_{ex} for the mode placed at 4.6 GHz compared to the two modes near 7.5 GHz and also satisfying $\kappa_{ex} << \omega$.

4.2.3 External Coupling via Impedance Transformer

The next challenge is to engineer the external coupling in such a way that the 4.6 GHz frequency mode is coupled stronger to the feedline compared to the other 2 modes. This hierarchy of κ_{ex} for the modes is achieved through the use of an impedance transformer. Using the theory discussed in section 1.9, an appropriate length for the transformer was selected to obtain the desired coupling fig. 4.6. The transformer has a characteristic impedance of 150 Ω, set by its width (10 μm). This, along with the combination of two capacitors selectively couples the lower frequency mode stronger to the output ports. The ratio of κ_{ex} for the modes was calculated by a fitting a Lorentzian around the simulated transmission curve peaks, the width of which, gives insight into the external decay rate.

Conclusion

This thesis work explored the phenomena of non-reciprocal dynamics in the context of microwave circuit optomechanics. We analysed the simplest multi mode optomechanical system capable of exhibiting non-reciprocal behavior. We showed that under appropriate conditions, the system can achieve very high levels of isolation. Although the bandwidth of non-reciprocity is narrow, this constraint can be overcome via reservoir engineering discussed in the next section. By suitably pumping an additional tone at the lower sideband, it is, in theory, possible to achieve high damping rates which can lead to higher bandwidth of non-reciprocity. In this regard, the circuit design shown in the main text is extremely versatile. It is possible to engineer the system to achieve reverse dissipation regime, ie, where the dissipation rate of the mechanical oscillator dominates that of the electromagnetic modes, and break reciprocal symmetry via balancing a coherent interaction(say using kinetic inductance) with the optomechanical one. Furthermore, the circuit can be modified very easily in such a way that the higher order mechanical mode is also coupled to the two primary electromagnetic modes and the cooling mode can be used to cool the oscillator. This will, in effect, produce similar results as the simple scheme discussed, but with a higher bandwidth. Such an implementation, without the use of external magnetic bias is promising in the context of quantum computing and information processing applications. The simplest scheme studied in this thesis can also be used, in theory, to realise interesting topological states. A square lattice of alternating microwave and EM modes, although difficult to realise, can produce frequency conversion only in the outer edges due to non-reciprocal behavior. In such a case, one mechanical mode will be coupled to four EM modes simultaneously in an array, possibly producing edge states.

A System Parameters

Here we list the parameters used for the numerical simulations of non-reciprocity schemes and the values of the components used in the circuit design. These values are closely related to those observed experimentally in

A.1 Mathematica Simulations

A.1 gives the parameters used in Mathematica numerical simulations for investigating various schemes for non-reciprocity. The optomechanical coupling strength g_0 is related to cooperativity $\mathscr{C}$ as

$$g_0 = \sqrt{\frac{\kappa\Gamma\mathscr{C}}{4}} \tag{A.1}$$

System Parameter	Value	Unit
ω_1	2π 4.13	GHz
κ_1	2π 200	kHz
$\kappa_{1,\mathrm{in}}$	2π 50	kHz
$\kappa_{1,\mathrm{ex}}$	2π 150	kHz
ω_2	2π 5.24	GHz
κ_2	2π 3300	kHz
$\kappa_{2,\mathrm{in}}$	2π 300	kHz
$\kappa_{2,\mathrm{ex}}$	2π 3000	kHz
Γ_1	2π 100	Hz
Γ_2	2π 200	Hz
Ω_1	2π 10.9	MHz
Ω_2	2π 6.5	MHz

Table A.1 – System parameters

System Variable	Value	Unit
L_1	2.2	nH
L_2	5	nH
C_c	10	fF
C_{ex}	60	fF
Other Inductors	5	nH
Other Capacitors	50	fF

Table A.2 – Parameters used in circuit design using Sonnet (fig. 4.1)

A.2 Sonnet Simulations

A.2 gives the parameters used in sonnet simulations. Superconducting aluminum used in the simulations has a width of 3 μm except in the case of the impedance transformer which has a width of 10 μm. This particular value was chosen to obtain a characteristic impedance of 150 Ω. The external feedline is 500 μm wide. The simulation was carried out in a 3 layered structure. The bottom layer is Sapphire with a thickness of 500 μm and the distance between 2^{nd} and 3^{rd} layers is 50 nm. The parallel plate capacitor has dimensions $17 \times 15\,\mu$m, chosen such that the capacitance is 50 fF.

Bibliography

[1] N. R. Bernier, L. D. Toth, A. Koottandavida, A. K. Feofanov, and T. J. Kippenberg. Nonreciprocal microwave transmission using circuit optomechanics. *arXiv:1612.08223*, 2016.

[2] A. Nunnenkamp, V. Sudhir, A. K. Feofanov, A. Roulet, and T. J. Kippenberg. Quantum-Limited Amplification and Parametric Instability in the Reversed Dissipation Regime of Cavity Optomechanics. *Physical Review Letters*, 113(2):023604, July 2014.

[3] L.D. Toth, N.R. Bernier, A Nunnenkamp, E. Glushkov, A.K. Feofanov, and T.J. Kippenberg. A dissipative quantum reservoir for microwave light using a mechanical oscillator. *arXiv:1602.05180 [cond-mat, physics:quant-ph]*, 2016.

[4] Max Born and Emil Wolf. *Principles of optics: electromagnetic theory of propagation, interference and diffraction of light.* CUP Archive, 2000.

[5] A. Metelmann and A. A. Clerk. Nonreciprocal photon transmission and amplification via reservoir engineering. *Physical Review X*, 5(2):021025, 06 2015.

[6] A. Metelmann and A. A. Clerk. Non-reciprocal quantum interactions and devices via autonomous feed-forward. *arXiv:1610.06621*, 10 2016.

[7] V.B. Braginsky, A.B. Manukin, and M. Yu. Tikhonov. Investigation of dissipative ponderomotive effects of electromagnetic radiation. *Sov. Phys. JETP*, 31(5):829, 1970.

[8] J.Aumentado and L. Ranzani. Graph-based analysis of nonreciprocity in coupled-mode systems. *New Journal of Physics*, 16(103027):10, 10 2014.

[9] K. M. Sliwa, M. Hatridge, A. Narla, S. Shankar, L. Frunzio, R. J. Schoelkopf, and M. H. Devoret. Reconfigurable josephson circulator/directional amplifier. *Phys. Rev. X*, 5:041020, Nov 2015.

[10] Kejie Fang, Jie Luo, Anja Metelmann, Matthew H. Matheny, Florian Marquardt, Aashish A. Clerk, and Oskar Painter. Generalized nonreciprocity in an optomechanical circuit via synthetic magnetism and reservoir engineering. *arXiv:1608.03620*, 08 2016.

[11] Freek Ruesink, Mohammad-Ali Miri, Andrea Alù, and Ewold Verhagen. Nonreciprocity and magnetic-free isolation based on optomechanical interactions. *Nature Communications*, 7(13662), 11 2016.

[12] T. J. Kippenberg, H. Rokhsari, T. Carmon, A. Scherer, and K. J. Vahala. Analysis of radiation-pressure induced mechanical oscillation of an optical microcavity. *Phys. Rev. Lett.*, 95:033901, Jul 2005.

[13] B.P Warwick and G. J. Milburn. *Quantum Optomechanics.* CRC Press, 10 2015.

[14] Markus Aspelmeyer, Tobias J. Kippenberg, and Florian Marquardt. Cavity optomechanics. *Reviews of Modern Physics*, 86(4):1391–1452, December 2014.

[15] C.W. Gardiner and M.J. Collet. Input and output in damped quantum systems: Quantum stochastic differential equations and the master equation. *Phy. Rev. A*, 31(6):3761, 06 1985.

[16] G. J. Milburn and D. F. Walls. *Quantum Optics.* Springer, 2008.

[17] I. Wilson-Rae, N. Nooshi, W. Zwerger, and T. J. Kippenberg. Theory of ground state cooling of a mechanical oscillator using dynamical backaction. *Phys. Rev. Lett.*, 99:093901, Aug 2007.

[18] J. D. Teufel, T. Donner, Dale Li, J. W. Harlow, M. S. Allman, K. Cicak, A. J. Sirois, J. D. Whittaker, K. W. Lehnert, and R. W. Simmonds. Sideband cooling of micromechanical motion to the quantum ground state. *Nature*, 475(7356):359–363, July 2011.

[19] A. Schliesser, R. Rivière, G. Anetsberger, O. Arcizet, and T. J. Kippenberg. Resolved-sideband cooling of a micromechanical oscillator. *Nat Phys*, 4(5):415–419, 05 2008.

[20] Florian Marquardt, Joe P. Chen, A. A. Clerk, and S. M. Girvin. Quantum theory of cavity-assisted sideband cooling of mechanical motion. *Phys. Rev. Lett.*, 99:093902, Aug 2007.

[21] C. Eichler, Y. Salathe, J. Mlynek, S. Schmidt, and A. Wallraff. Quantum-limited amplification and entanglement in coupled nonlinear resonators. *Phys. Rev. Lett.*, 113:110502, Sep 2014.

[22] Hanna Krauter, Christine A. Muschik, Kasper Jensen, Wojciech Wasilewski, Jonas M. Petersen, J. Ignacio Cirac, and Eugene S. Polzik. Entanglement generated by dissipation and steady state entanglement of two macroscopic objects. *Phys. Rev. Lett.*, 107:080503, Aug 2011.

[23] Katarina Cicak, Dale Li, Joshua A. Strong, Michael S. Allman, Fabio Altomare, Adam J. Sirois, Jed D. Whittaker, John D. Teufel, and Raymond W. Simmonds. Low-loss superconducting resonant circuits using vacuum-gap-based microwave components. *Applied Physics Letters*, 96(093502), 2010.

[24] G. Anetsberger, E. M. Wieg, J. P. Kotthaus, and T. J. Kippenberg. Cavity optomechanics and cooling nanomechanical oscillators using microresonator enhanced evanescent near-field coupling. *Comptes Rendus Physique*, 12(9-20):800–816, 12 2011.

[25] Thomas Corbitt, David Ottaway, Edith Innerhofer, Jason Pelc, and Nergis Mavalvala. Observation of critical coupling in a fiber taper to a silica-microsphere whispering-gallery mode system. *PHYSICAL REVIEW A*, 74:021802, 2006.

[26] Archana Kamal. *Nonreciprocity in active Josephson junction circuits.* PhD thesis, Yale University, 03 2013.

[27] K. M. Sliwa, M. Hatridge, A. Narla, S. Shankar, L. Frunzio, R. J. Schoelkopf, and M. H. Devoret. Reconfigurable josephson circulator/directional amplifier. *Phys. Rev. X*, 5:041020, Nov 2015.

[28] F. Lecocq, J. B. Clark, R. W. Simmonds, J. Aumentado, and J. D. Teufel. Mechanically mediated microwave frequency conversion in the quantum regime. *Phys. Rev. Lett.*, 116:043601, 01 2016.